ATOMIC WEAPONS ESTABLISHMENT

AWE REPORT NO. O 2/89

Broad-Band P Wave Seismograms of Six Underground Explosions in the USA Recorded at a Selection of LRSM Stations

R C Lilwall
J B Young

Recommended for issue by

A Douglas, Superintendent

Approved by

B L Elphick, Head of Division

CONTENTS

SUMMARY

This report presents seismograms from six explosions recorded at selected stations operated as part of the Long Range Seismic Measurements (LRSM) Project. Four of the explosions (BILBY, BOXCAR, GREELEY and PILEDRIVER) were fired at the Nevada Test Site (NTS), one (SHOAL) at the Sand Springs Range Nevada, and one (SALMON) in the Tatum salt dome near Hattiesburg, Mississippi. In general three types of seismogram are shown: the vertical short-period (SP) seismogram, the broad-band (BB) seismogram, and the BB seismogram corrected for anelastic attenuation. Most of the recordings are at regional distances (less than 30^{o}) and the influence of upper mantle and crustal structure results in complex seismograms. It is shown that the P_n waveform at distances of a few degrees can be reproduced in theoretical seismograms. Estimates of the amplitude of the reduced displacement potential of the explosions are made from the pulse area of the initial P pulse from teleseismic recordings and from the amplitude of the BB P_n arrival. The estimates using P_n show similar scatter to the teleseismic estimates but show better agreement with values predicted from close-in "free field" measurements.

1. INTRODUCTION

The estimation of the yields of nuclear explosions using seismological methods is important in the verification of compliance with a Threshold Test Ban Treaty. In some recent publications (1,2,3,4,5) the use of Broad-Band (BB) recordings is investigated as an alternative to the use of the conventional short and long period (SP and LP) passbands in yield estimation. The attraction of using BB recordings is that much more of the source spectrum is included in the waveforms and therefore yield estimates should be more stable than those obtained from narrow band recordings. Yield estimation using BB recordings is generally made through the estimation of the long term level ψ_{inf} of the reduced displacement potential $\psi(t)$ (abbreviated to RDP and related to both observed near and far field displacements). It is hoped that ψ_{inf} estimates will relate to yield more reliably than empirical measures of source size as the various magnitude scales in normal use. Evaluation of the use of BB recordings and the use of ψ_{inf} will require many observations for explosions of known yield.

In this report a sample of BB seismograms are produced from recordings made under the Long Range Seismic Measurements (LRSM) program operated under the VELA-UNIFORM project during the 1960s. The basic data are digital SP seismograms produced from the original analogue LRSM recordings. The six explosions considered represent a wide range of both yield and source media which are unlikely to be repeated in future US tests. The largest explosions (BILBY, BOXCAR and GREELEY) were high yield and fired in tuff at the Yucca Flats and Pahute Mesa regions of NTS. Two explosions (SHOAL and PILEDRIVER) were in granite and one (SALMON) in salt.

The BB seismograms at teleseismic distances are used in this report to estimate values of ψ_{inf} using established techniques (1). It is

hoped that such ψ_{inf} values will be a useful addition to the sparse number available at present in the literature.

At present negotiations about a Threshold Test Ban have concerned relatively high yields (150 kton) and seismological verification using observations at teleseismic distances. In the verification of compliance with any future Low Yield Threshold Test Ban, poor signal-to-noise ratio at stations at teleseismic distances will make it necessary to use data from stations near to a test site. Any method of yield estimation using data from stations at short range is clearly of interest and it will be seen that BB recordings of the P_n phase observed at ranges of a few hundred kilometres may be useful, at least for NTS. Within the constraints provided by the known source parameters of the explosions, unlike the teleseismic P phase, most features of the P_n arrival appear to be explained using a simple theoretical model. Much of this report is concerned with the use of P_n in yield estimation.

2. PROCESSING METHODS

The processing methods used are similar to those described in Lyman, Douglas, Marshall and Young (1). The data consist of vertical SP seismograms digitised at 20 samples per second from the original LRSM analogue recordings. The BB seismograms are obtained by passing the SP seismograms through a filter with a response $|a_2(\omega)|/a_1(\omega)$, where $a_1(\omega)$ and $a_2(\omega)$ are the response of the SP and BB instruments as a function of angular frequency ω.

To remove high and low frequency noise which may interfere with the signals of interest all the seismograms have been bandpass filtered between 0.25 to 4.0 Hz and following Lyman et al (1) Wiener frequency filtering (Douglas and Young (6)) used to suppress noise around the signal frequency. The latter are designed using the noise spectrum observed before the signal and simple assumptions about the signal spectrum. The filters used are two sided which helps to preserve pulse shape but their acausality can result in precursors to the initial onset.

Corrections for the effect of anelastic attenuation are applied by passing the seismograms through a filter with a response $(b(\omega))^{-1}$, where $b(\omega)$ is the response as a function of frequency of an attenuation operator. In this report the attenuation operator of Carpenter (7) is used, where $|b(\omega)|$ is exp $(-\omega t^*/2)$ and the phase specified using the theory of Futterman (8). This procedure is probably valid for observations at "teleseismic" distances (greater than approximately 30°) where all the observed seismic arrivals follow essentially similar paths. A t* value of 0.35 s is used in this report to correct for teleseismic paths from NTS as suggested by the work of Lyman et al (1). Seismograms in the range 10 to 30° show multiple arrivals resulting from the upper mantle structure and clearly the assumption of a single path is not valid. In the absence of noticeable frequency differences between most of the arrivals however, a single t* operator is used. Values of t* in excess of 0.35 s are required to fully correct predominantly upper mantle paths out of NTS but the presence of noise in the data generally precludes their use here. An upper limit of 0.35 s is therefore used and many of the seismograms remain under-corrected for anelastic attenuation. At distances less than about 10° several distinct crustal phases are usually present and the use of a simple t* operator is invalid. For completeness, however, a t* value assumed to be appropriate for the first arrival (P_n)

phase is applied, that is using an upper mantle Q of 200 for the Nevada explosions and 500 for SALMON. For the Nevada explosions the assumed t* value rises from 0.1 s at 200 km to 0.35 s at 600 km.

3. SEISMOGRAMS

Figures 1 to 6 show the "P wave" seismograms for the six explosions, the data in each set arranged in the order of increasing distance. For each seismogram the time period has been centred on the first visible P arrival. Accurate calibrations of the amplitudes are not available but approximate calibrations have been made using the measured amplitudes of the P arrivals published in the shot reports (25-30). For some seismograms misidentification of the exact phase measured in the report is possible and may result in incorrect calibration. Table 2 gives the amplitudes corresponding to the vertical bars down the centre of each figure.

The majority of the seismograms are from stations at "far regional" distances (between 10 to 30°, 1100 to 3300 km) and are characterised by multiple arrivals representing triplications orginating from the 400 and 700 km upper mantle discontinuities. For this reason the SP records have been used by several workers (9,10,11) to investigate the upper mantle structure. The influence of structure on both pulse shapes and amplitudes means that seismograms of the initial P wave arrival(s) from this distance range are difficult to use in the study of the source itself. The BB seismograms often have differences both in the character and prominence of phases compared with the SP records. They are presented here for completeness and in the hope that further insight may be obtained concerning the upper mantle structure. Reinterpretation of the seismograms at the far regional distance range is beyond the scope of this report.

At the few stations at "teleseismic" distances (ie, in excess of approximately 30°) the P pulse shapes have many features in common with those published in Lyman et al (1) for Nevada to Eskdalemuir (EKA) paths. The t* corrected record of PILEDRIVER at NPNT (figure 4) displays all the features observed at EKA; two pulses of opposite polarity and separated by 0.8 s. The separation is far too long to identify the second phase as pP from the known depth of the source and as yet no satisfactory explanation is available in terms of a simple explosion source model (Douglas and Rivers (12)). The BB seismograms for the large Pahute Mesa explosions BOXCAR (at HNME and SV3QB see figure 2c) and GREELEY (at HNME see figure 3b) all show three main phases similar to those tentatively identified as P, pP and A_s (a possible "slapdown" arrival) on EKA records (1). For the Yucca Flats explosion BILBY the BB record at NPNT (figure 1d) also shows features similar to that at EKA, ie, a smaller "slapdown" phase followed by an additional unidentified arrival. The records for SHOAL (EUAL, DHNY, LSNH, HNME in figure 6d) are too noisy for comment on pulse shapes but are used in section 5 below to obtain approximate estimates of source size ψ_m. At NPNT the BB record for SALMON (figure 5c) shows a clear double pulse of 0.8 s duration. Complexity of the pulse shape is likely for an explosion detonated in a salt dome which has a 3D velocity structure with strong contrasts across boundaries. The PcP arrival is also shown in figure 5c and here the first arrival pulse 0.3 s long is resolved, presumably because of the greater separation of the phases for the more steeply travelling PcP path.

The most extensive data at "near regional" distances (0 to 10°) are for the Pahute Mesa explosion BOXCAR (figure 2a, b). In general the initial BB P_n arrival consists of a positive pulse 0.6 to 1.0 s duration when measured on the t* corrected seismograms. The seismograms for BILBY and GREELEY (figures 1a and 3a) also have these characteristics but for the two explosions in granite PILEDRIVER and SHOAL (figures 4 and 6a) the pulse lengths are much shorter (0.3 to 4 s). Complexity of the waveforms makes it difficult to identify a negative pP arrival on the MNNV and KNUT seismograms for PILEDRIVER comparable to the phase present on teleseismic seismograms. If the P_n arrivals represent head-waves then in the absence of interfaces other than the Moho the BB pulse shape represents RDP of the source. In the absence of overshoot in the RDP the BB P "pulse" should be long and have a step-like appearance. The effect of any overshoot and the surface reflection pP will be to produce more pulse-like arrivals as is observed. Normal shot firing procedures result in source sizes which tend to increase with depth of burial. Since both time to the RDP maximum and pP-P time also similarly increase a correlation of pulse length and depth of burial is expected. The short pulse lengths for the two shallow SHOAL and PILEDRIVER compared with the deeper BILBY, GREELEY and BOXCAR fit this but clearly a much larger sample will be required to confirm whether useful information is present in these observations.

4. THEORETICAL SEISMOGRAMS OF THE P_n PHASE

Werth, Herbst and Springer (13) show that the amplitude of the "first half cycle" of the P_n phase of some explosions at NTS can be predicted from the "free field" displacement observed near the source and a simplified theoretical model to account for the effects of reflection, refraction and attenuation in the structure beneath source and station. It is of interest to see if any of the features observed in the BB seismograms at near regional distances can also be reproduced using more recent techniques to produce theoretical waveforms.

Figures 7 to 9 show some theoretical vertical component BB seismograms calculated using the method described by Kennett (14) which is applicable for point sources situated in a plane layered half-space. The seismic velocity structure is based on the Basin and Range Structure of Priestley and Brune (15) with essentially a two-layered crust 35 km thick above a 7.8 km/s upper mantle. The top 5 km of superficial layering used varies depending on the part of the NTS being considered (see table 3). Anelastic attenuation is taken into account using values of Q, assumed to be frequency independent, based on the results of Patten and Taylor (16). Source time histories used are computed using the model of Mueller and Murphy (17). Kennett's method involves an integration for the response of the structure as a function of slowness. The integration has no upper limit but since this report is concerned primarily with the P waves the integration has been restricted to the slowness range 0.0 to 0.2 s/km. The method assumes a flat earth and to obtain accurate results at the largest distance an earth flattening transformation was applied to all the velocity structures considered (Aki and Richards (33)). The same band pass filter (0.25 to 4.0 Hz) used with the observed seismograms was applied to the theoretical waveforms.

For PILEDRIVER a velocity gradient is used in the superficial layering as given in table 3, structure A. This gives the observed average uphole velocity of near 4.5 km/s. Figure 7 (left and centre) shows the theoretical seismograms for the P_n and P_g phases for a range of

distances using source functions based on the known yield of 62 kton and also for a reduced yield of 20 kton. The simple positive P_n pulses observed at MNNV and KNUT are reproduced in the theoretical results but the short duration is only reproduced with a source waveform corresponding to 20 kton yield. The uniform upper mantle results in a stable pulse shape for P_n but even with a simple crustal structure the form of the P_g arrivals vary with distance. There is some similarity however, between the first two seconds of the P_g group starting about 1.2 s after P_n on the observed BB seismogram at MNNV and the theoretical waveforms at similar distances but the low frequency of the arrival is not predicted. An improved fit to the MNNV observation is seen in the theoretical seismograms in figure 7 (right), and results from reducing the depth of the intermediate crustal layer interface from 25 to 15 km. The low frequency phase (a head-wave from the lower crustal layer) is now visible because of the relative delay introduced to the sharp supercritical Moho reflection PmP which produces a prominent negative arrival which appears to start the P_g group on the SP record.

Douglas and Rivers (12) show that both the teleseismic P waveforms together with the Love and Rayleigh wave radiation from PILEDRIVER are compatible with a predominantly double-couple source situated 2 to 3 km below the shot point. It is of interest to see whether such a source is compatible with the P_n waveforms observed at MNNV and KNUT (figure 4). Figure 8 shows the theoretical waveforms using the azimuth and distance ranges appropriate to MNNV and KNUT for the preferred double-couple mechanism suggested by Douglas and Rivers (12) and assuming an impulsive source time history. The P_n waveforms are a poorer fit to the observations than those produced in figure 7 using an explosion mechanism at the correct depth. The delay in the pP arrival introduced by the 2.5 km source depth results in BB P_n pulses which are much longer than observed. At KNUT the very long P_n pulse arises because the source radiation pattern gives only a low amplitude pP, and sP terminates the phase. It appears that the P_n waveforms at MNNV and KNUT do not support the hypothesis that the seismic radiation from PILEDRIVER is primarily tectonic release induced by the explosion.

Figure 9 shows the theoretical seismograms for the BILBY and BOXCAR explosions using superficial layering corresponding to Yucca Flats and Pahute Mesa respectively as given in table 3, structures B and C. Use of the known source parameters for GREELEY results in theoretical seismograms which, apart from the amplitudes, are similar in form to those for BOXCAR shown in figure 9. Although the Yucca and Pahute explosions are at very different firing depths, there is little difference in the expected pP-P times and this results in similar theoretical BB P_n pulse shapes. It will be seen in the next section that the main effect of the strong velocity contrast at the palaeozoic boundary beneath Yucca Flats is to reduce the amplitudes with respect to those obtained using the more gradational Pahute structure. Comparison of the theoretical waveforms with those observed in figures 1 to 3 (where signal-to-noise ratio permits) reveals that the P_n waveforms are reproduced and that the best agreement is at the smallest distances where it extends to the initial arrival of the P_g group (eg, BILBY at CUNV, BOXCAR and GREELEY at MNNV).

5. SOURCE PARAMETERS

5.1 Teleseismic data

The source function of explosions can be defined by the reduced displacement potential $\psi(t)$. After one or two seconds $\psi(t)$ rapidly approaches a constant value ψ_{inf} which is usually assumed to be proportional to yield. The far-field displacement is proportional to the time derivative $\psi'(t)$. An estimate of ψ_{inf} can be obtained from the area under the initial P pulse after correction for differences in medium properties at the source and beneath the station, geometrical spreading and the effect of the free surface at the station.

Using the BB seismograms from stations at teleseismic distance from the sources ψ_{inf} estimates in this report are made by multiplying pulse areas by $[2G(\Delta)]^{-1}(\rho_o v_o/\rho_i v_i)^{\frac{1}{2}}$ where $G(\Delta)$ is the geometrical spreading term given by Carpenter (18), ρ_i and v_i are the density and P wave speed at the source, ρ_o and v_o are the density and speed at the receiver.

The station NPNT recorded a clear PcP arrival from SALMON which has a more distinct first arrival pulse than the P wave. Using the geometrical spreading and core/mantle reflection coefficients for PcP published by Carpenter (18) an additional estimate of ψ_m for SALMON has been made. It will be seen that this estimate is consistent with other P wave values and PcP data may be valuable where earth structure degrades the initial P arrival.

There are three principal sources of error in such estimates: firstly the interference of the direct P with the surface reflection pP; secondly the presence of low frequency noise may effect the area measurement; and thirdly at distances less than about 30^o upper mantle structure can have a strong influence both on pulse shape and amplitude, hence the geometrical spreading correction terms are either not available or may be inappropriate. A further problem arises if the RDP overshoots to a maximum value ψ_{max} before falling back to the final value ψ_{inf} as sometimes observed in free field observations and incorporated in some models of the explosion source (17,19). Interference from other phases, especially pP, means that any source overshoot is difficult to observe unambiguously, and pulse area measurements probably reflect the value of ψ_{max} rather than ψ_{inf}. Since it is not usually possible to make the distinction, references to ψ_{max} and ψ_{inf} will henceforth be grouped and abbreviated ψ_m.

ψ_m measurements based on pulse areas are included in table 4 for recordings at distances greater than 24^o, the brackets around some estimates are cautionary because of the epicentral distance (less than 30^o) and/or poor signal-to-noise ratio.

5.2 Near regional data

Werth, Herbst and Springer (13) show that the amplitude of the first half cycle of the P_n arrival on SP instruments at distances between 300 to 600 km can be predicted assuming classical head-wave theory, from the RDP measured near the source. In the previous section it is demonstrated that many features of the BB P_n arrival are reproduced using theoretical seismograms based on a simple earth model, thus confirming the

observations of Werth et al (13). The BB P_n observations seem potentially useful for the measurement of ψ_m and the remainder of this section describes an estimation procedure.

If the P_n arrival is a true head wave then its form represents the RDP $\psi(t)$ and not the time derivative $\psi'(t)$, hence the amplitude not the area of the pulse is the appropriate measure of ψ_m. Estimates of ψ_m have therefore been made for stations at distances between 180 and 700 km which have a measurable BB P amplitude. To obtain ψ_m the measured amplitudes must be corrected using distance factors to allow for geometrical spreading and anelastic attenuation.

Distance factors were obtained using the P_n amplitude decay measured on theoretical BB seismograms computed in the same way as those illustrated in figures 7 to 9 and described in the previous section. The structures A, B and C in table 3 are used for the NTS explosions, structure D for the SALMON event is based on that used by Springer (2). Source waveforms were computed assuming the Mueller-Murphy (17) explosion source model and representative yields and emplacement depths. For Yucca these are 10 and 100 kton at 0.3 and 0.6 km, and for Pahute 100 and 1000 kton at 0.6 and 1.2 km depth respectively. For the granitic structure A the depth was fixed at 0.5 km for yields of 20 and 50 kton and 0.3 km for 10 kton. For the SALMON model, a yield of 5 kton and a depth of 0.8 km is used, these values being close to the actual yield and depth. These source waveforms are used so that the interfering phases such as pP and the effect of anelastic attenuation are properly taken into account in the resulting amplitude variation. Kennett's method (14) does not allow for differing structures beneath the source and recording station and for the Yucca and Pahute structures the very low velocity materials are not representative of that beneath most stations with the result that the theoretical amplitudes will tend to be high. Apart from those applicable to the SALMON event, the P_n amplitudes have therefore all been corrected so as to correspond to a common station with 2 km of 4 km/s material overlying the 6.1 km/s basement. This was done by deconvolving the P_n waveforms with the response of the original station layering and then convolving with the common alternative assuming that the P_n phase represents a plane wave with apparent velocity equal to the sub-Moho P wave speed. For the SALMON event a near surface P wave speed of 2.7 km/s, known to be present beneath station JELA, is assumed (see Der, McElfresh and Mrazek (21)). The largest changes occur with the theoretical P_n amplitudes for Yucca which are reduced by a factor of approximately 2. The measured P_n amplitudes (in nanometres) are plotted as a function of epicentral distance Δ in figures 10 to 13. They are normalised to correspond to a source with ψ_m of 1 m^3 and can be used to convert observed BB P_n amplitudes measured in nanometres to estimates of ψ_{max} in m^3. All the curves have the same general form with an inverse power decay varying with the range $\Delta^{-2.85}$ and $\Delta^{-3.25}$ for NTS and $\Delta^{-2.25}$ for the SALMON structure. In the absence of appreciable velocity gradient below the Moho the theoretical decay resulting from geometrical spreading and elastic propagation for the head wave is approximately $\Delta^{-2.0}$ (eg, Cerveny and Ravindra (22)). The contribution due to anelasticity is clearly appreciable for the NTS structures (Q upper mantle = 200) compared with that used for SALMON (Q set to 500).

Comparison of the curves for the NTS structures reveals the relatively efficient transmission out of the granitic structure A compared with the Yucca Flats which has the strong velocity contrast at the

Palaeozoic boundary. The amplitude factors for NTS vary by a factor of 2 and clearly a knowledge of the local layering at the source is required to enable accurate estimation of ψ_m.

Table 4 includes the ψ_m values estimated from the BB P_n amplitudes and the distance factors in figure 10 to 12 are listed in table 5.

5.3 Discussion

Figures 14 and 15 show the "teleseismic" and "near regional" ψ_m estimates plotted against the published yields (23). The teleseismic values have been augmented with values obtained for the station EKA by Lyman et al (1) and for YKA by Gillbanks, Marshall and Stewart (5) and Marshall (24). Plotted values from the latter publications have all been corrected for differences in seismic wave speeds and densities at the source and beneath the receiver. Anomalously high ψ_m values obtained with the station UBO for GREELEY and BOXCAR suggest that here the first P arrival is not a head wave and these two points are not plotted. Figure 16 shows the magnitudes obtained from the published P_n amplitude and period data published in the LRSM shot reports (25 to 30) and using formulae obtained by Evernden (31).

The regression lines fitted in figures 14 and 15 show that the variation of ψ_m with yield is similar for both the teleseismic and P_n estimates. The teleseismic estimates are, however, a factor of approximately 5 low compared with both those derived from the P_n data and those predicted from the Mueller-Murphy model (17). Since the latter is in part based on observed free field RDP measurements it appears that the discrepancy results from the teleseismic estimates being too low. A similar but smaller difference has been noted by McLaughlin, Lees, Der and Marshall (4) in their ψ_m estimates for French explosions in Southern Algeria. There are several possible explanations of these observations:-

(a) The free field RDP data may overestimate the far field values because of non-linear behaviour near the measurements. To this may be added the possibility that the RDP may not be spherically symmetric with the result that near field measurements made to the side of explosions do not represent the values corresponding to downgoing radiation.

(b) Defocussing of the small sample of teleseismic data.

(c) Interference with the pP arrival.

(d) Underestimation of the effect on the teleseismic pulse area of losses due to scattering, reflections and conversions in the crust and upper mantle.

(e) Use of incorrect t* values to allow for anelastic attenuation because Q may be frequency dependent.

The agreement of the ψ_m estimates from P_n with the free field data would appear to discount (a) above. Focussing and defocussing effects (b) tend to average out with large networks but may well be important if the small and poorly distributed observations for the NTS are defocussed. The teleseismic data are strongly biased by observations from

the eastern USA, and from a similar azimuth to EKA. Defocussing may lead to bias with this small sample from the focal sphere. It is noticeable that the ψ_m estimates from the two stations YKA and NPNT not to the east are on the top side of the regression line in figure 14 and if these were typical of values from a more extensive network the discrepancy would be reduced, but not eliminated. The effect of pP (c) is very difficult to assess because of the likelihood of non-linear behaviour in the region above the source. In addition phases observed on records and interpreted as pP are frequently delayed from that expected. Reduction in the measured P pulse area seems inevitable but is difficult to quantify. McLaughlin et al (4) indicate that hypothesis (d) is unlikely by itself to account for the 30 to 50% amplitude reductions apparent in their data for Southern Algeria. The area of separate pulse-like arrivals is insensitive to the value of t* assumed, but if several arrivals produce an oscillatory waveform, however, both the value of t* used and the assumed frequency independence may result in bias to the measured areas and hence ψ_m. In this context, McLaughlin et al suggest that a frequency dependence of t* amounting to $dt^*/df = 0.2$ Hz/s at 1 Hz could account for all of the discrepancy found in their results for Southern Algerian explosions. The acceptance of any model in support of any frequency dependence of Q, however, awaits confirmation from both frequency and time domain observations.

Comparison of figures 14 and 15 shows that the ψ_m estimates based on the BB P_n data have advantages in yield determination when compared with the use of magnitude based on SP log(A/T) measurement. For individual explosions the ψ_m estimates appear less scattered than the magnitudes. Moreover, the ψ_m estimates are a better fit to the regression line. For SHOAL and PILEDRIVER, both in granite, the respective under and overestimation present in the magnitudes, are not evident with ψ_m.

Near regional data will become important in the verification of any future low yield threshold test ban where teleseismic data may not be available because of poor signal-to-noise ratio. The use of BB P_n data seems promising, at least from the NTS observations. The success with this data arises because the structure below the Moho in the region around the test site is a good approximation to a uniform half space down for at least 20 to 30 km. At greater depths or laterally this may not be so and the assumption that P_n is a head-wave will give erroneous results (ie, station UBO possibly). Figure 13 includes distance factors computed for alternative upper mantle structures to that used for NTS. The "high gradient" structure is the NTS granitic structure A in table 3 with the uniform upper mantle replaced with a gradient model rising by 1.0 km/s over 100 km. The amplitudes diverge from those found with a uniform upper mantle beyond 200 km range and remain constant beyond 300 km. In the presence of high gradients the P_n phase ceases to be a true head-wave and both the amplitude decay and waveform are not predicted by simple theory (eg, Cerveny and Ravindra (22)). A structure based on observational data in western Europe is represented by that published by Kind (32). Here the upper mantle has a fine structure with alternating low and high velocity regions with velocity changes of up to 0.4 km/s over 10 to 20 km depth ranges. This type of structure has a profound effect on the seismograms and the amplitude distance factors based on the first BB peak have an irregular distance dependence. As with the high-gradient upper mantle the overall amplitude fall-off with distance is much slower than with a uniform upper mantle. One effect of the enhanced P_n amplitudes is to make the P_g crustal arrival less prominent, as is observed with near regional seismograms in the eastern USA. Clearly the general use of P_n data to

determine yield will require extensive calibration to determine the amplitude decay to stations around the test site. In general the P_n data with the highest amplitude (and it is hoped signal-to-noise ratio) are at the shortest distances and it is fortunate that at distances up to about 250 km range all the upper mantle structures studied here produce P_n amplitudes with a smooth distance decay. At greater distances, irregular amplitude variation, even with plane layered structures may limit the value of the phase for yield estimation.

6. ACKNOWLEDGEMENTS

The LRSM digital data used in this report were made available through the data services section of Teledyne Geotech, Alexandria, Virginia. Thanks are also due to A Douglas and P D Marshall at Blacknest for many helpful discussions and suggestions concerning the work in this report.

REFERENCES

1. N S Lyman, A Douglas, P D Marshall, J B Young: "P Seismograms Recorded at Eskdalemuir, Scotland from Explosions in Nevada, USA". AWRE Report O 10/86, HMSO, London (1986)

2. R C Stewart: "P-wave Seismograms from Underground Explosions at the Shagan River Test Site Recorded at Four Arrays". AWE Report O 4/88, HMSO, London (1988)

3. I G Stimpson: "Source Parameters of Explosions in Granite at the French Test Site in Algeria". AWE Report O 11/88, HMSO, London (1988)

4. K L McLaughlin, A C Lees, Z A Der, M E Marshall: "Teleseismic Spectral and Temporal M_Q and ψ_∞ Estimates for Four French Explosions in Southern Algeria". Bull Seism Soc Am, 78, 4, 1580-1596 (1988)

5. T G A Gillbanks, P D Marshall, R C Stewart: "P-wave Seismograms Recorded at Yellowknife, Canada from Underground Nuclear Explosions in Nevada, USA". AWE Report O 26/88, HMSO, London (1988)

6. A Douglas, J B Young: "The Estimation of Seismic Body Wave Signals in the Presence of Oceanic Microseisms". AWRE Report O 14/81, HMSO, London (1981)

7. E W Carpenter: "Absorption of Body Waves - An Operator for a Constant Q Mechanism". AWRE Report O 43/66, HMSO, London (1966)

8. W I Futterman: "Dispersive Body Waves". J Geophys Res, 67, 5279-5291 (1962)

9. C B Archambeau, E A Flinn, D G Lambert: "Fine Structures of the Upper Mantle". J Geophys Res, 74, 5825-5866 (1969)

10. D Helmberger, R A Wiggins: "Upper Mantle Structure of Midwestern United States". J Geophys Res, 76, 3229-3245 (1971)

11. L J Burdick, D V Helmberger: "The Upper Mantle P Velocity Structure of the Western United States". J Geophys Res, 83, 1699-1712 (1978)

12. A Douglas, D W Rivers: "An Explosion that Looks Like an Earthquake". Bull Seism Soc Am, 78, 2, 1011-1019 (1988)

13. G C Werth, R F Herbst, D L Springer: "Amplitudes of Seismic Arrivals from the M Discountinuity". J Geophys Res, 67, 1, 1587-1609 (1962)

14. B L N Kennett: "Seismic Waves in a Stratified Half Space". Geophys J R Astr Soc, 61, 1-10 (1980)

15. K Priestley, J Brune: "Surface Waves and the Structure of Nevada and Western Utah". J Geophys Res, 83, 2265-2272 (1978)

16. H J Patton, S R Taylor: "Q-structure of the Basin and Range from Surface Waves". J Geophys Res, 89, 6929-6940 (1984)

17. R A Mueller, J R Murphy: "Seismic Characteristics of Underground Nuclear Detonations". Bull Seism Soc Am, 65, 1675-1692 (1971)

18. E W Carpenter: "A Quantitative Evaluation of Teleseismic Explosion Records". Proc Roy Soc A, 290, 396-407 (1966)

19. D von Seggern, R Blandford: "Source Time Functions and Spectra for Underground Nuclear Explosions". Geophys J R Astr Soc, 31, 83-97 (1972)

20. D L Springer: "Calculation of First-zone P-wave Amplitudes for Station Event and for Decoupled Sources". J Geophys Res, 71, 3459-3467 (1966)

21. Z A Der, T W McElfresh, C P Mrazek: "The Effect of Crustal Structure on Station Magnitude Anomalies (Magnitude Bias)". Report SDAC-TR-77-1 (1977)

22. V Cerveny, R Ravindra: "Theory of Seismic Head-Waves". University of Toronto Press (1971)

23. US Department of Energy: "Announced United States Nuclear Tests: July 1945 through December 1984". Report NVO-209 (Rev 5). Office of Public Affairs, US Dept of Energy, Nevada Operations Office (1985)

24. P D Marshall: Personal Communication

25. Long Range Seismic Measurements Project 8.4 BILBY. ARPA Project VELA-UNIFORM, Datdc Report 87 (1963)

26. Long Range Seismic Measurements Project 8.4 SHOAL. ARPA Project VELA-UNIFORM, Datdc Report 92 (1963)

27. Long Range Seismic Measurements Project 8.4 SALMON. ARPA Project VELA-UNIFORM, Seismic Data Lab Report 113 (1964)

28. Long Range Seismic Measurements Project PILEDRIVER. ARPA Project VELA-UNIFORM, Seismic Data Lab Report 165 (1966)

29. Long Range Seismic Measurement Project GREELEY. ARPA Project VELA-UNIFORM, Seismic Data Lab Report 180 (1967)

30. Long Range Seismic Measurements BOXCAR. ARPA Project VELA-UNIFORM, Seismic Data Lab Report 223 (1968)

31. J F Evernden: "Magnitude Determination at Regional and Near Regional Distances in the United States". Bull Seism Soc Am, 57, 591-639 (1967)

32. R Kind: "Long Range Propagation of Seismic Energy in the Lower Lithosphere". Z Geophys, 40, 189-202 (1974)

33. K Aki, P G Richards: "Quantitative Seismology: Theory and Methods". Freeman, San Francisco (1980)

Shot	DATE	TIME	LAT	LONG	YIELD kt	DEPTH m	MED	Vp km/s	RHO
BILBY	130963	17-00-00	37 03'38"N	116 01'18"W	249	714	TUFF	2.4	1.9
BOXCAR	260468	15-00-00	37 17'44"N	116 27'21"W	1300	1158	RHYOLITE	3.4	2.2
GREELEY	201266	15-30-00	37 18'07"N	116 24'30"W	870	1215	TUFF	3.4	2.2
PILEDRIVER	020666	15-30-00	37 13'37"N	116 03'20"W	62	463	GRANITE	5.5	2.7
SALMON	221064	10-00-00	31 08'32"N	89 34'12"W	5	828	SALT	4.4	2.2
SHOAL	261063	17-00-00	39 12'01"N	118 22'49"W	12	367	GRANITE	5.0	2.7

TABLE 1. Details of the six explosions studied in this report.

	STN	Seismogram			STN	Seismogram		
	CODE	1	2	3	CODE	1	2	3
Shoal	MNNV	39200	31800	38000	WINV	3360	5890	7800
	MVCL	11900	5540	12300	CUNV	9280	5960	12000
	KNUT	587	381	2282	HLID	814	447	4500
	CPCL	153	734	--	BXUT	229	217	--
	DRCO	59	88	--	TKWA	62	125	--
	TDNH	31	42	--	LCNM	50	87	--
	SKTX	240	169	--	RYND	274	174	--
	APOK	50	116	--	HHND	246	307	--
	DUOK	227	155	--	EBMT	114	110	--
	RKON	118	113	--	LVLA	108	157	--
	EUAL	110	156	357	DHNY	40	43	142
	LSNH	28	63	147	HNME	45	81	224
Piledrver	MNNV	67700	49200	71100	KNUT	12000	16400	24600
	WMSD	962	2030	4910	WMO	112	454	817
	KCMO	599	1160	3110	NPNT	409	658	1980
Bilby	CUNV	80000	133000	162000	CPCL	9620	14200	30300
	WINV	3640	1620	6500	BXUT	6180	5410	18700
	DRCO	1620	1450	5830	HLID	2190	1770	7400
	TDNM	573	1040	2420	RTNM	216	349	863
	LCNM	181	271	720	AZTX	808	2030	3850
	FRMA	2460	9620	19300	TKWA	346	1210	2020
	SKTX	393	2190	3670	GIMA	722	2690	5690
	RYND	2220	4760	8780	GVTX	1490	6440	12500
	DUOK	565	2050	3850	HHND	2064	7220	13400
	HETX	496	1940	3610	EBMT	7860	3920	6920
	RKON	1280	3840	7340	BLWV	225	586	1340
	BRPA	193	562	1200	NPNT	668	2590	5120
Greeley	MNNV	483600	616000	712900	KNUT	232600	424100	673200
	TFO	6280	16500	29600	MOID	9100	29900	55800
	UBO	17800	41300	85600	FKCO	2450	5030	10400
	WMO	1470	10518	17300	KCMO	2150	15600	24300
	PGBC	4250	21900	36800	RKON	4800	21600	37900
	CPO	1000	2760	5310	HNME	1400	7400	12800
Boxcar	MNNV	648000	780000	987000	BPCL	--	--	--
	ATNV	302000	199000	351000	EYNV	288000	412000	625000
	BFCL	16500	37200	50500	KGAZ	246000	465000	674000
	NDCL	109000	168000	241000	KNUT	334000	400000	597000
	CPCL	16400	20600	49000	UBO	34100	37000	99200
	LCNM	1030	2390	4850	PGBC	4340	19100	35500
	RKON	3540	15800	30500	WH2YK	392	1830	3050
	HNME	1200	6050	10700	SV3QB	830	3110	5690
Salmon	EUAL	4190	2260	2780	JELA	16500	13000	15600
	GVTX	666	327	--	BRPA	105	76	--
	WFMN	141	79	--	DRCO	17	59	--
	GPMN	91	66	--	NLAZ	37	55	--
	GEAZ	37	116	--	WOAZ	41	94	--
	HRAZ	38	80	--	LGAZ	25	83	--
	SNAZ	24	65	--	RKON	86	74	--
	SGAZ	47	87	--	EKNV	14	24	--
	HLID	12	43	--	MNNV	9	19	42
	NPNT	65	135	193	NPNT	43	180	105

NB Factors give the amplitude in nanometres represented by the vertical Bars in figs 1-6. For the SP records (seismograms 1) a frequency of 1 Hertz is assumed

Table 2. Amplitude Factors for Seismograms in Figs 1-6

	Vp km/s	Vs km/s	Rho g/cc	Q	Thickness km
A. NTS Granitic	4.5	2.6	2.6	50	0.2
	5.0	2.7	2.7	50	0.2
	5.5	2.9	2.7	50	0.5
	6.1	3.5	2.8	300	24.0
	6.6	3.8	2.8	300	10.0
	7.8	4.5	3.3	200	Half Space
B. NTS Yucca Flats	1.8	1.0	1.8	50	0.5
	2.4	1.3	1.9	50	0.5
	5.3	2.9	2.8	100	4.0
	6.1	3.5	2.8	300	20.0
	6.6	3.8	2.8	300	10.0
	7.8	4.5	3.3	200	Half Space
C. NTS Pahute Mesa	2.3	1.2	1.9	50	0.5
	2.7	1.55	2.0	50	0.3
	3.4	1.95	2.2	100	1.1
	4.4	2.53	2.5	100	0.5
	5.1	2.93	2.7	100	2.5
	6.1	3.5	2.8	300	20.0
	6.6	3.8	2.8	300	10.0
	7.8	4.5	3.3	200	Half Space
D. Salmon structure	1.9	0.9	2.0	50	0.25
	5.0	3.0	2.5	50	0.20
	4.4	2.5	2.2	50	3.2
	4.8	2.7	2.3	500	2.5
	6.0	3.6	2.8	500	11.0
	6.8	4.1	3.0	500	19.6
	8.3	4.6	3.38	500	Half Space
E. High Gradient	Same as A above but with 7.8 km/s Half Space replaced with velocity gradient of 0.1/s approximated by layers every 3km for 15km then every 5km.				
F. After Kind(32)	4.0	Vs = Vp / 1.74		50	2.0
	6.0	Rho= 1.7+0.2Vp		500	16.0
	6.5	Q based on Vp		500	17.0
	8.1	after (9)		400	6.5
	8.0			300	5.0
	7.9			200	7.0
	8.0			300	5.0
	8.1			400	3.25
	8.2			450	3.5
	8.1			400	2.0
	8.0			300	3.75
	8.1			400	5.0
	8.2			450	5.0
	8.3			500	3.75
	8.35			600	1.75
	8.3			500	2.25
	8.2			450	2.25
	8.1			400	2.25
	8.0			300	3.0
	8.2			450	4.25
	8.4			700	4.0
	8.2			450	2.0
	8.0			300	Half Space

Table 3. Crustal Structures Used for Theoretical Seismograms.

Shot code	Stn code	Dist km	Azim deg	BB	mb	Amplitude*	Dist fact+	Log10 ψm (m3)
BILBY	CUNV	186	15	196	5.29	19400nm	0.173	5.04
BILBY	CPCL	482	184	4	6.12	1775nm	0.0102	5.24
BILBY	WINV	492	346	165	5.24	621nm	0.00956	4.81
BILBY	BXUT	586	83	267	5.57	564nm	0.00577	4.99
BILBY	BLWV	3056	78	279	5.5	475nms	(0.021)	(4.35)
BILBY	BRPA	3236	73	276	5.6	500nms	(0.019)	(4.42)
BILBY	NPNT	4372	359	176	5.8	1000nms	0.012	4.92
BOXCAR	MNNV	195	311	130	6.16	87500nm	0.229	5.58
BOXCAR	ATNV	249	348	167	6.76	53895nm	0.0993	5.73
BOXCAR	EYNV	255	23	203	6.29	35083nm	0.0922	5.58
BOXCAR	BFCL	282	230	49	5.61	5424nm	0.0701	4.89
BOXCAR	KGAZ	293	128	310	6.64	(19375)nm	0.0630	(5.49)
BOXCAR	NDCL	310	164	345	5.74	10500nm	0.0552	5.28
BOXCAR	KNUT	324	94	276	6.58	28333nm	0.0506	5.75
BOXCAR	CPCL	507	179	359	6.03	4291nm	0.0154	5.44
BOXCAR	UBO	686	59	243	7.30	12333nm	0.00626	6.29
BOXCAR	WH2YK	2913	339	145	5.78	923nms	(0.031)	(4.47)
BOXCAR	HNME	4086	60	274	6.44	2393nms	0.017	5.15
BOXCAR	SV3QB	4199	46	263	6.10	1422nms	0.016	4.95
GREELEY	MNNV	198	310	129	6.25	82133nm	0.219	5.57
GREELEY	KNUT	320	94	277	6.44	24739nm	0.0519	5.68
GREELEY	TFO	572	124	307	6.26	1719nm	0.0108	5.20
GREELEY	MOID	641	1	181	5.61	(1180)nm	0.00772	(5.18)
GREELEY	UBO	682	58	243	7.13	8604nm	0.00639	6.13
GREELEY	CPO	2759	85	283	6.11	(980)nms	(0.034)	(4.46))
GREELEY	HNME	4082	60	274	6.42	2526nms	0.017	5.17
PILEDRIVER	MNNV	228	307	125	5.98	8405nm	0.178	4.67
PILEDRIVER	KNUT	288	94	275	5.63	2050nm	0.0962	4.32
PILEDRIVER	NPNT	4353	359	176	5.72	250nms	0.021	4.08
SALMON	EUAL	242	41	222	4.67	700nm	0.150	3.67
SALMON	JELA	243	288	106	4.97	1115nm	0.149	3.87
SALMON	MNNV	2725	295	99	3.84	(8.3)nms	(0.039)	(2.33)
SALMON	NPNT	5264	351	145	5.05	20.3nms	0.018	3.05
SALMON	NPNT(PcP)		345	145		5.5nms	0.0036	3.18
SHOAL	WINV	251	18	198	4.62	1162nm	0.112	4.02
SHOAL	MVCL	252	271	89	4.69	875nm	0.110	3.90
SHOAL	CUNV	260	102	284	4.36	313nm	0.0991	3.50
SHOAL	KNUT	544	115	298	4.66	(50)nm	0.0113	(3.65)
SHOAL	HLID	602	34	216	4.40	21nm	0.00834	3.40
SHOAL	EUAL	2828	95	293	5.1	46nms	0.043	3.03
SHOAL	DHNY	3652	70	280	4.8	17nms	0.026	2.81
SHOAL	LSNH	3856	66	278	5.0	33nms	0.024	3.14
SHOAL	HNME	4133	62	278	4.6	16nms	0.023	2.84

*Here 'Amplitude' is the height of the first arrival BB Pn pulse in nm for stations at distances less than 700km. At Teleseismic distance the amplitude is the area of the BB P pulse in nms.

+The geometrical spreading factors are in units of $(m^{-2})*10-9$ for Pn amplitudes and $(sm^{-2})*10-9$ for the P pulse areas. The latter are based on those of Carpenter(18) assuming $(\rho_0, v_0)=(2.4,4.0)$ & values in table 1 for (ρ_1, v_1) at each explosion

Table 4. Measured amplitudes and ψm estimates from the LRSM SP to BB converted seismograms.

Dist km	Yucca 10kt 0.3km	Yucca 100kt 0.6km	Pahute 100kt 0.6km	Pahute 1000kt 1.2km	Granite 50kt 0.5km	Granite 20kt 0.5km	Granite 10kt 0.3km	Salmon 5kt 0.8km
180	0.167	0.206	0.269	0.314	0.889	0.790	0.679	0.436
190	0.129	0.151	0.207	0.245	0.552	0.446	0.415	0.346
200	0.109	0.131	0.171	0.213	0.373	0.324	0.296	0.286
210	0.0911	0.112	0.143	0.187	0.282	0.243	0.211	0.234
220	0.0788	0.0991	0.123	0.158	0.218	0.202	0.180	0.211
240	0.0568	0.0693	0.0889	0.110	0.151	0.143	0.127	0.151
260	0.0433	0.0530	0.0693	0.0862	0.128	0.114	0.0991	0.132
280	0.0345	0.0443	0.0580	0.0715	0.113	0.105	0.0863	0.111
300	0.0279	0.0338	0.0470	0.0584	0.0937	0.0829	0.0713	0.0918
350	0.0194	0.0255	0.0327	0.0423	0.0521	0.0480	0.0394	0.0588
450	0.00808	0.0121	0.0148	0.0219	0.0250	0.0232	0.0188	0.0329
500	0.00615	0.00908	0.0114	0.0159	0.0182	0.0171	0.0138	0.0270
550	0.00457	0.00710	0.00816	0.0121	0.0144	0.0133	0.0110	0.0223
600	0.00334	0.00525	0.00606	0.00904	0.0111	0.0101	0.00840	0.0196
700	0.00193	0.00320	0.00365	0.00581	0.00700	0.00628	0.00530	0.0143

Table 5. BB Pn distance correction factors for various structures and source waveforms determined by yield & shot depth. Values are in metres squared x 10-9.

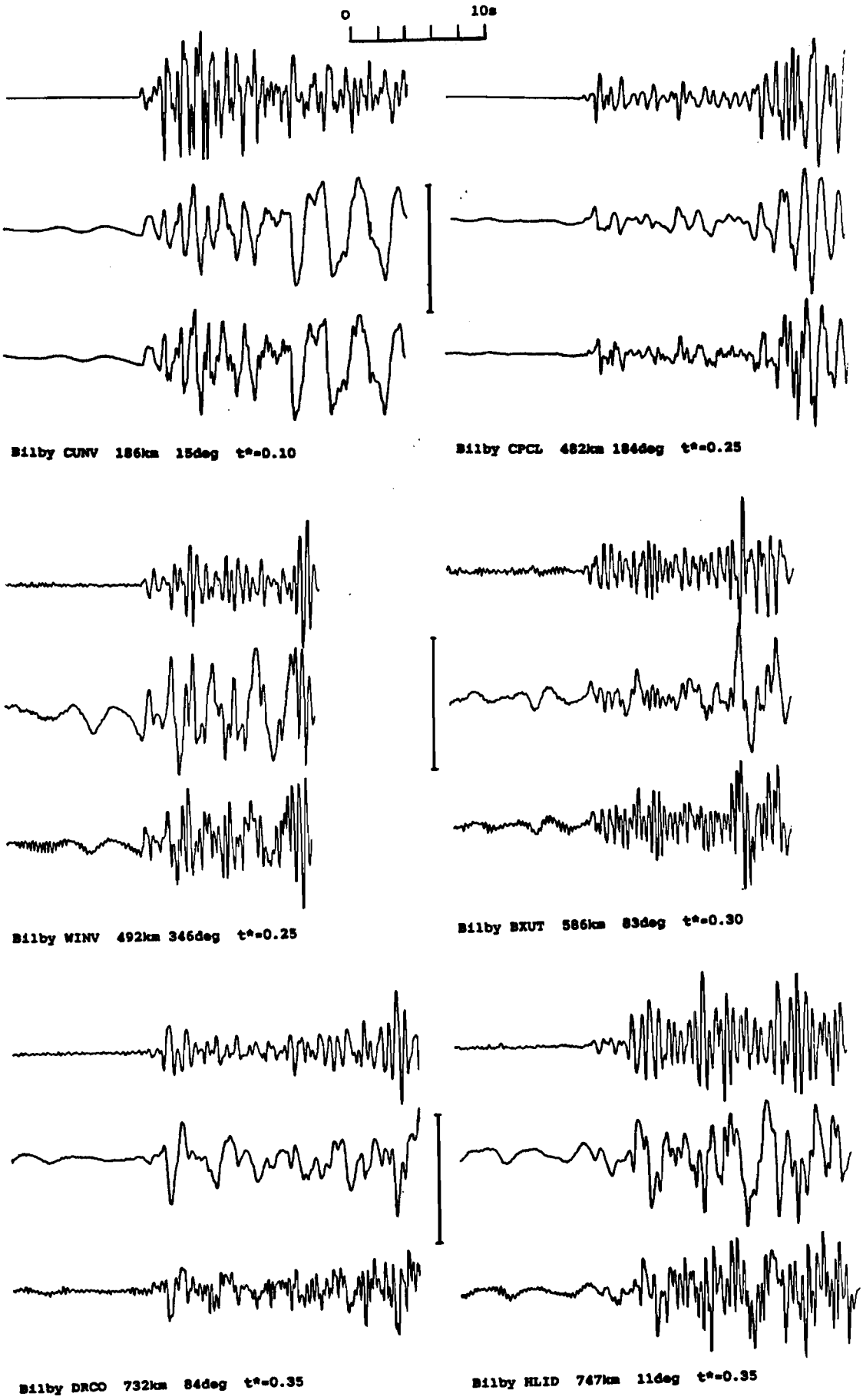

Fig 1a. SP,BB & t* corrected BB seismograms for BILBY

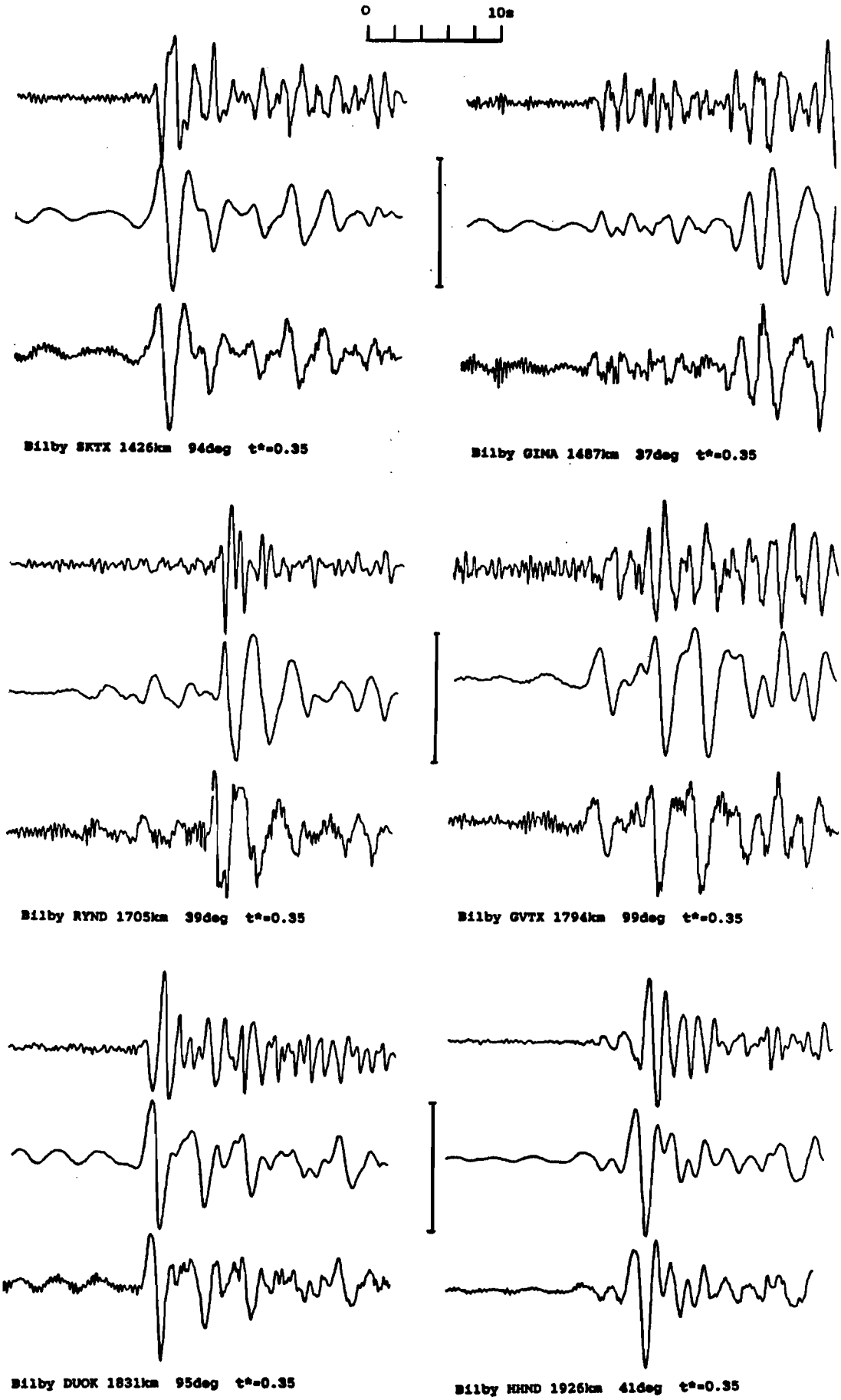

Fig 1c. SP,BB & t* corrected BB seismograms for BILBY

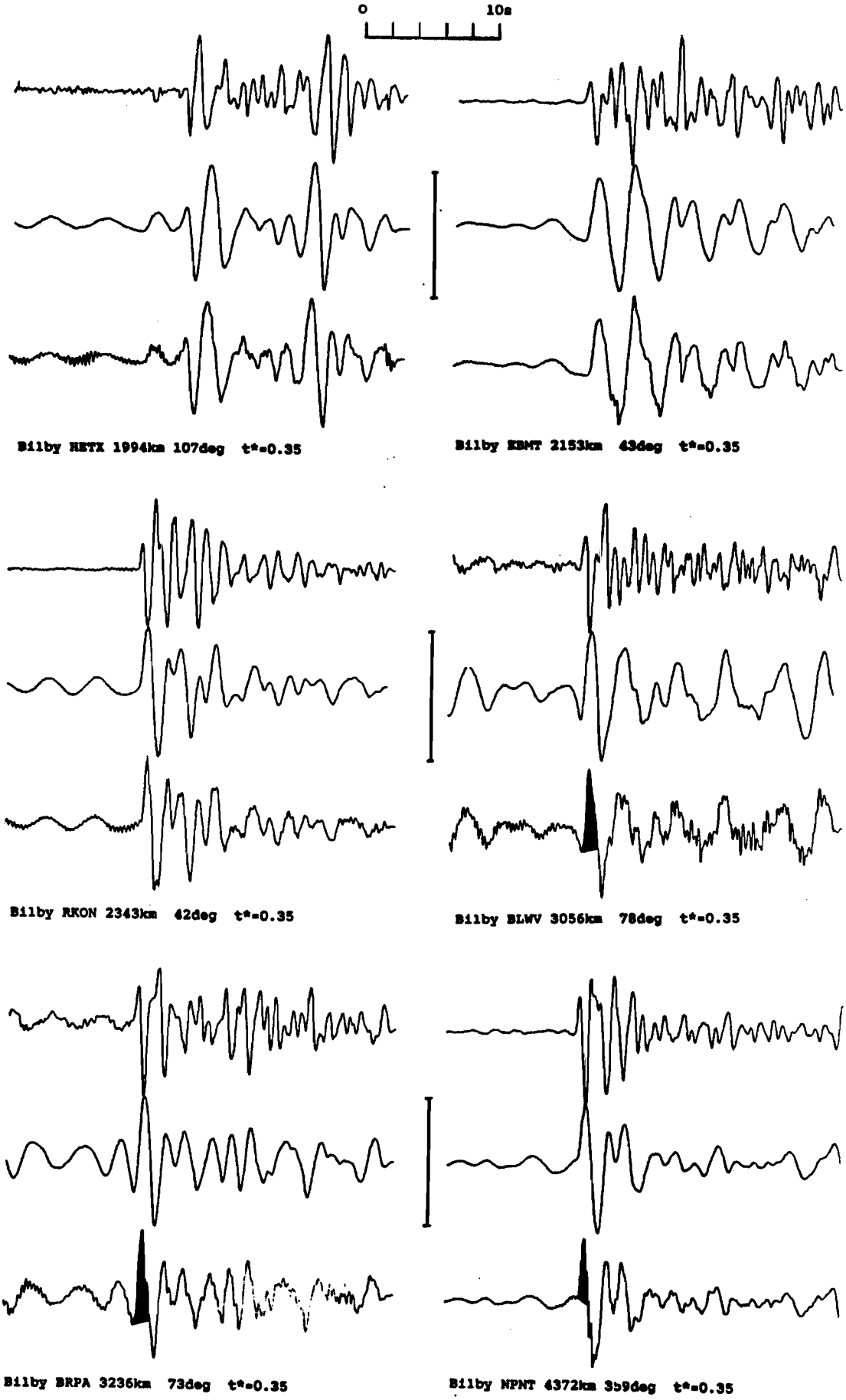

Fig 1d. SP,BB & t* corrected BB seismograms for BILBY

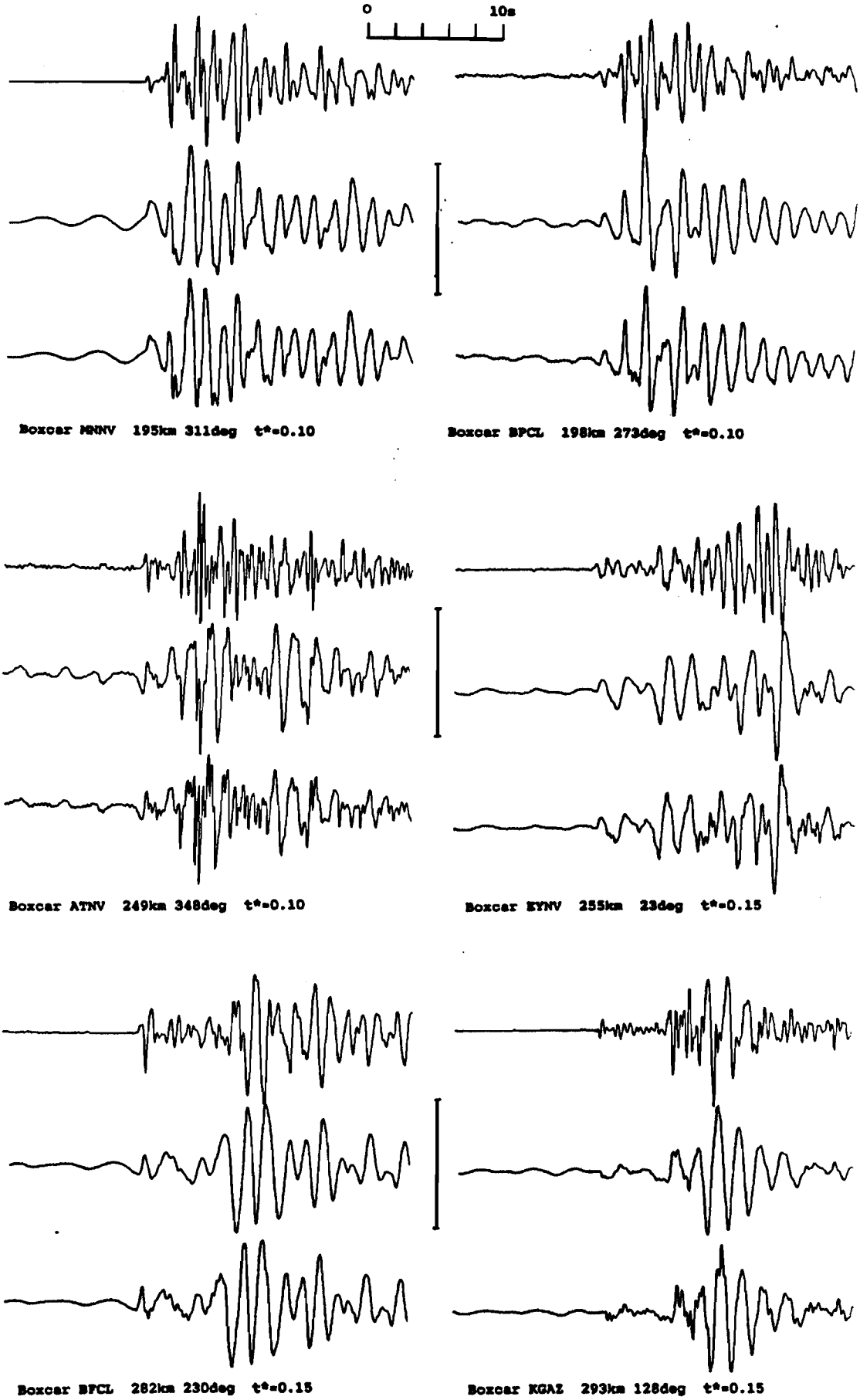

Fig 2a. SP,BB & t* corrected BB seismograms for BOXCAR

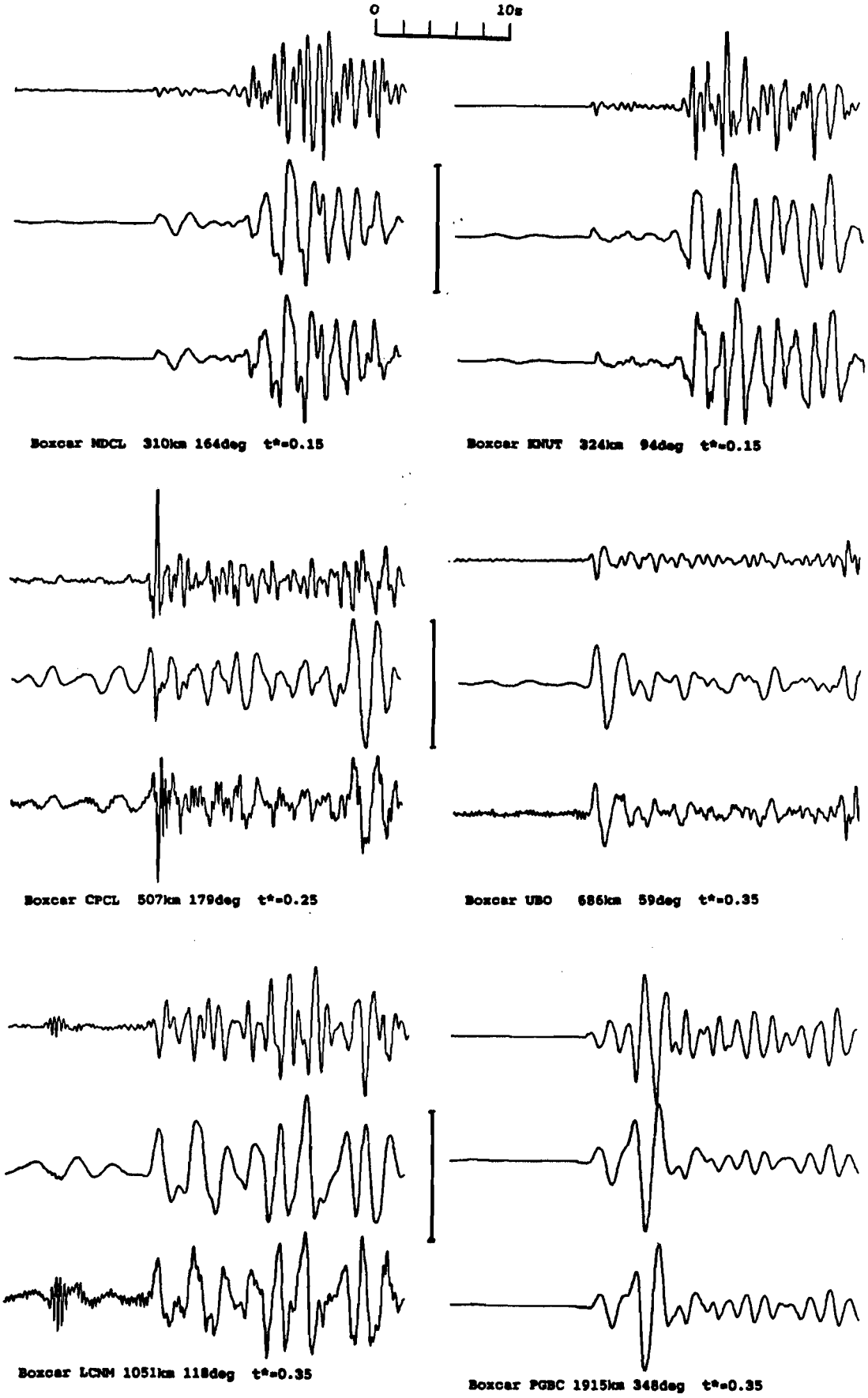

Fig 2b. SP,BB & t* corrected BB seismograms for BOXCAR

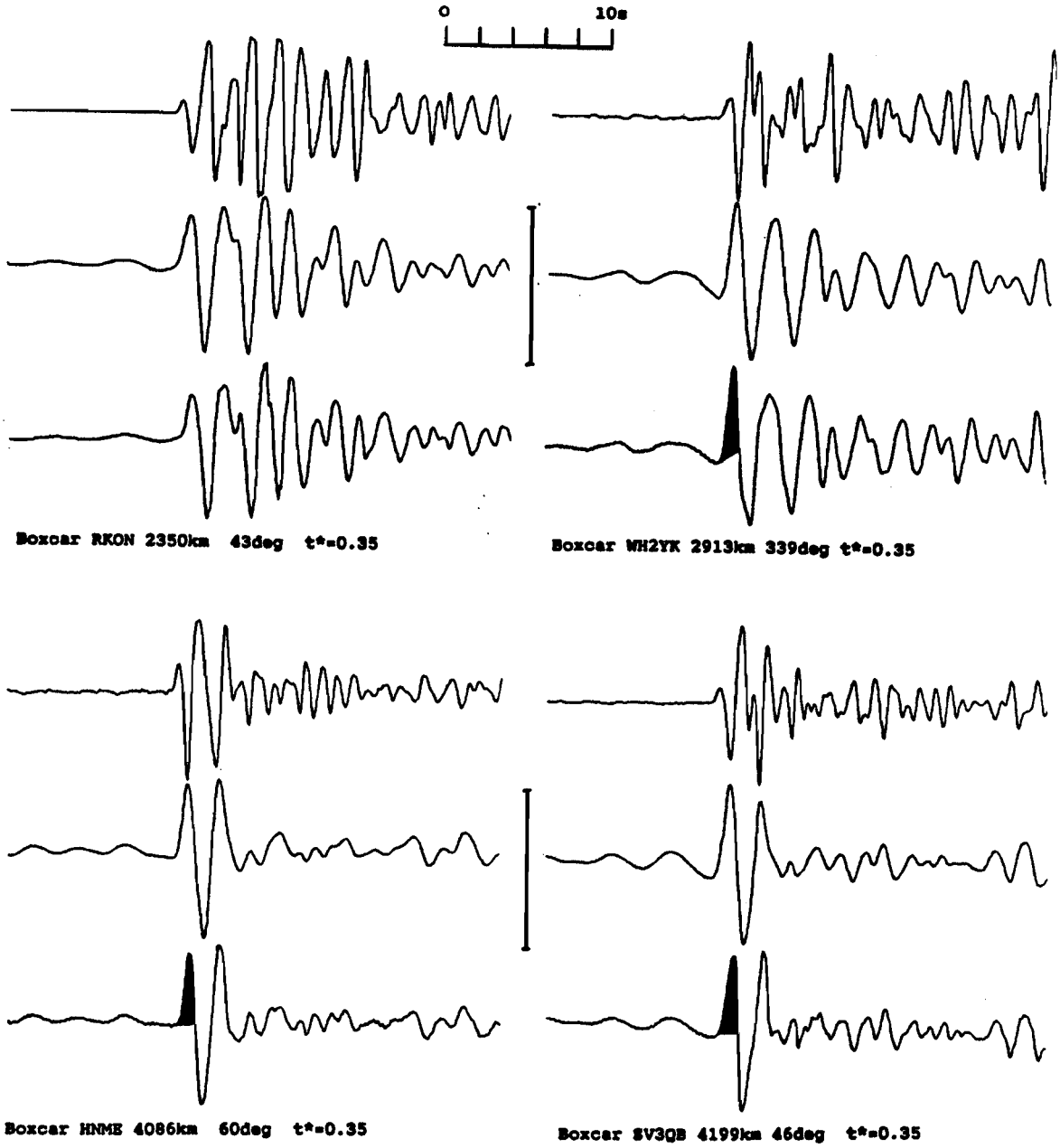

Fig 2c. SP,BB & t* corrected BB seismograms for BOXCAR

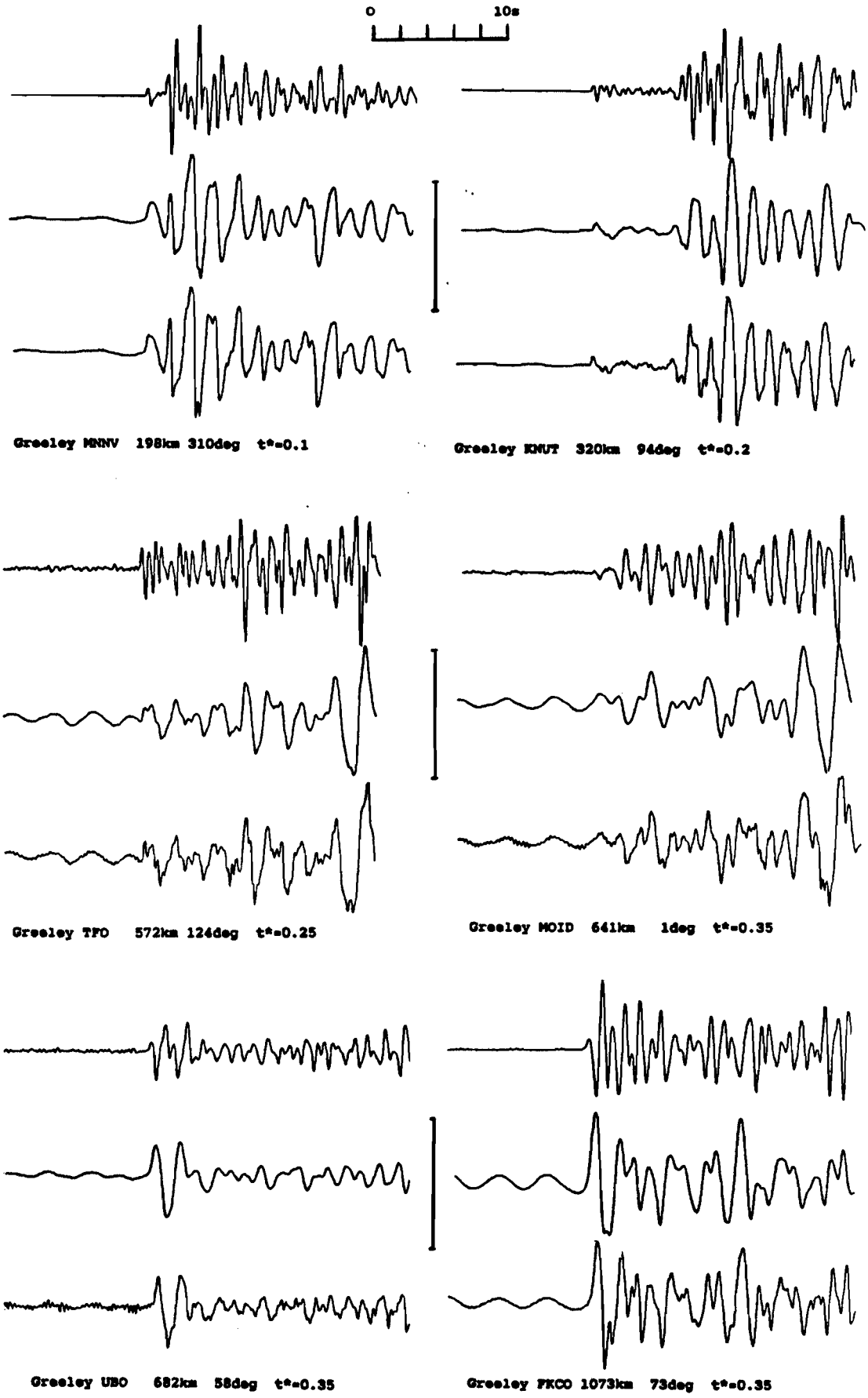

Fig 3a. SP,BB & t* corrected BB seismograms for GREELEY

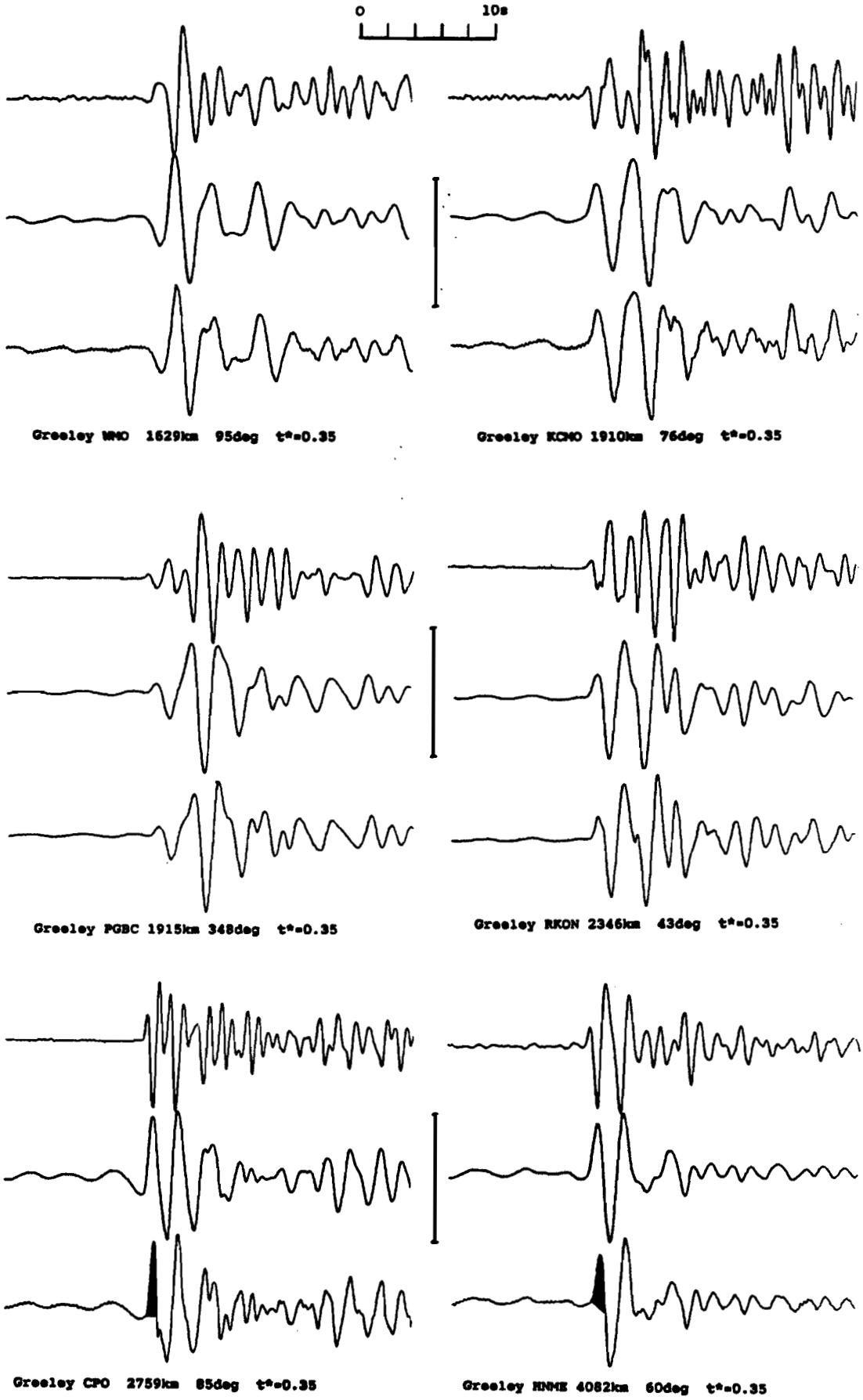

Fig 3b. SP,BB & t* corrected BB seismograms for GREELEY

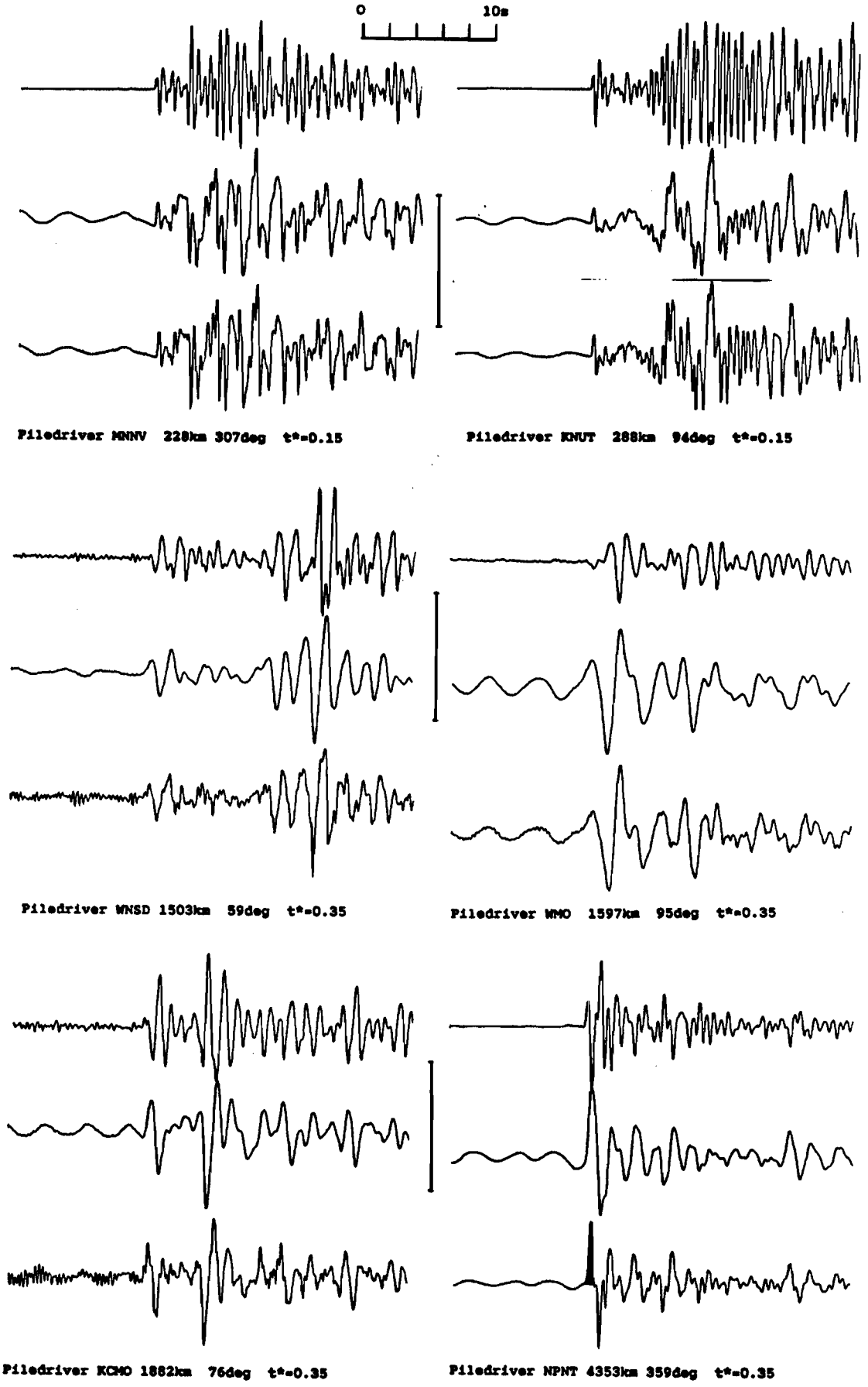

Fig 4. SP,BB & t* corrected BB seismograms for PILEDRIVER

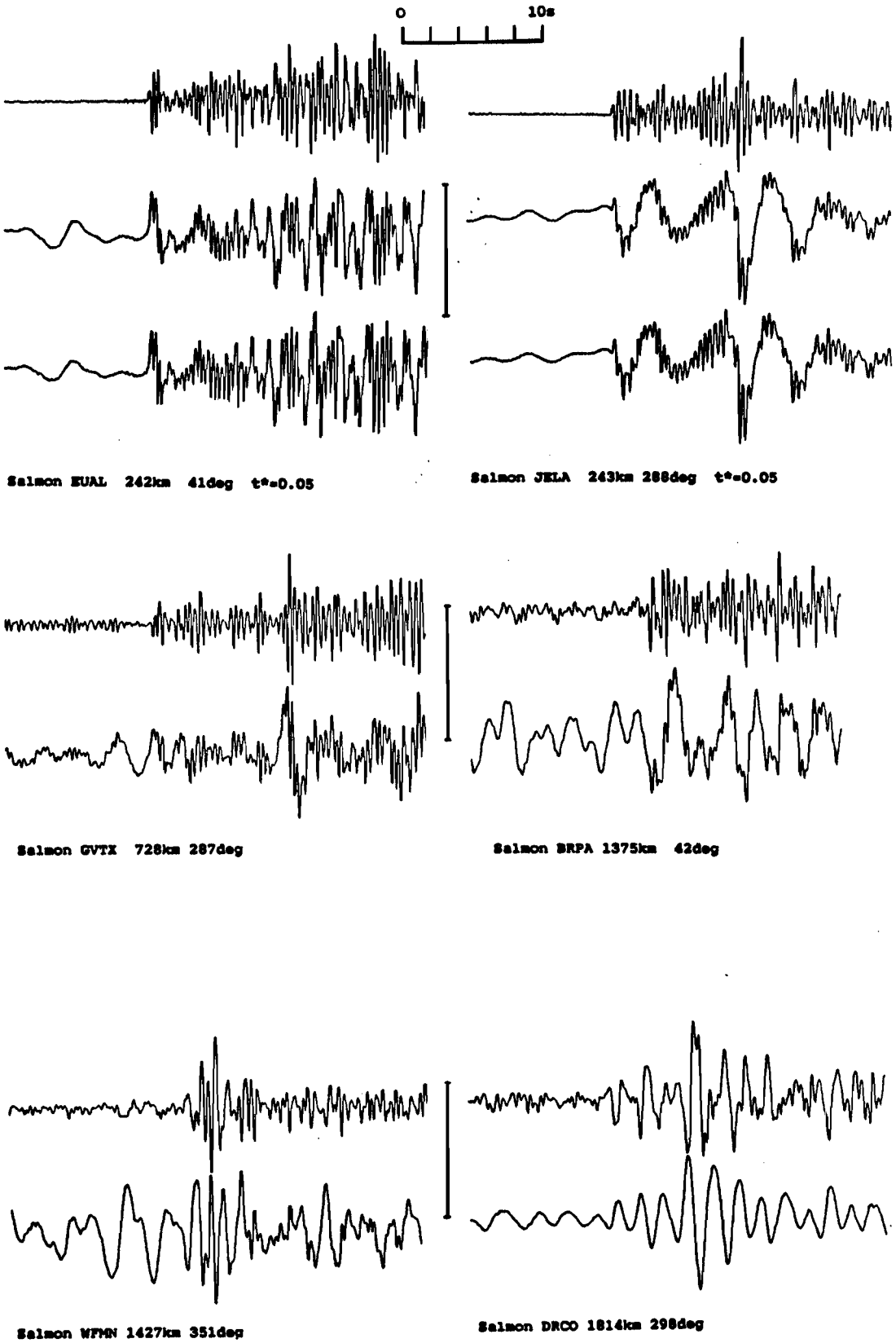

Fig 5a. SP,BB & t* corrected BB seismograms for SALMON

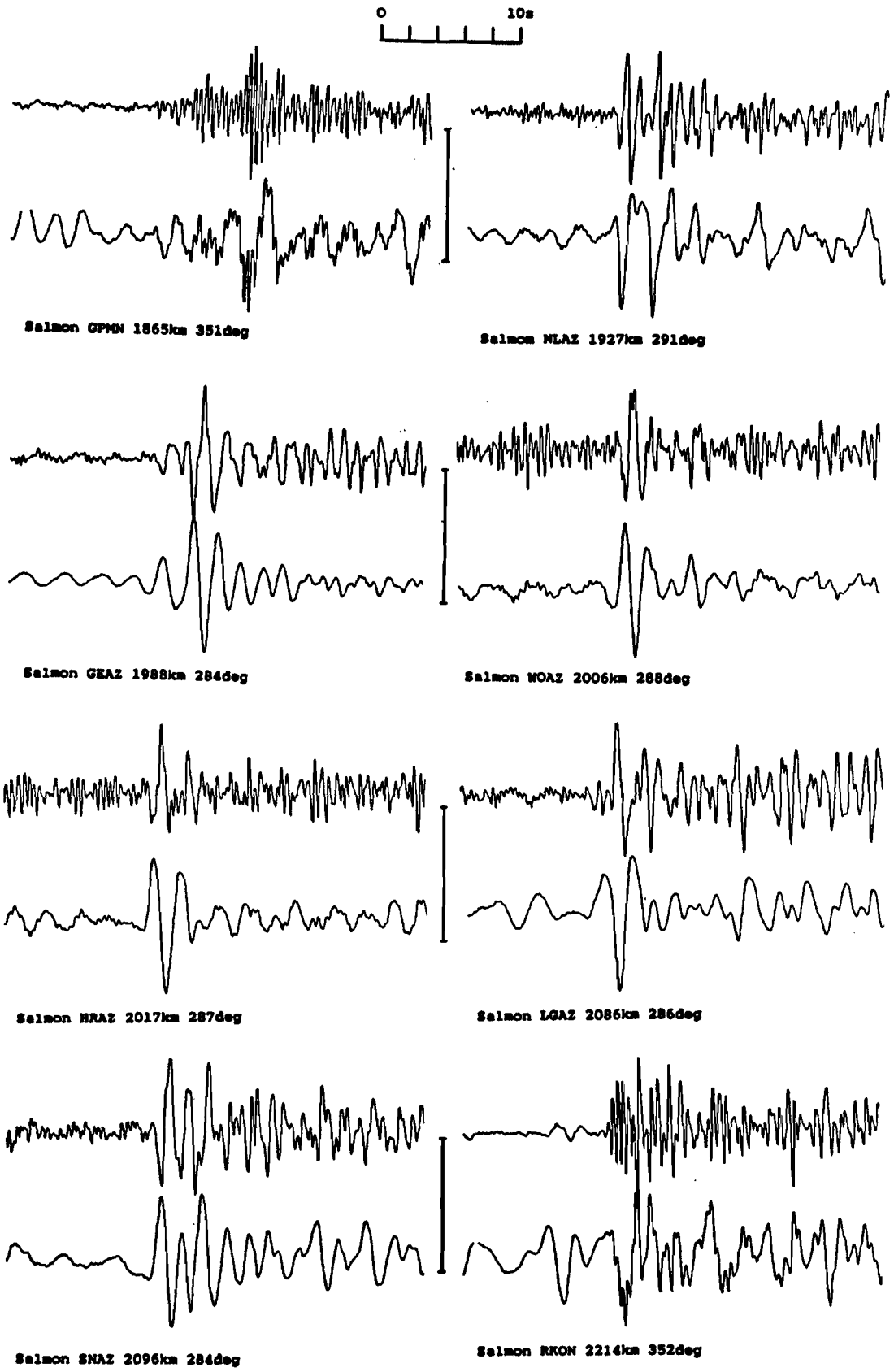

Fig 5b. SP,BB & t* corrected BB seismograms for SALMON

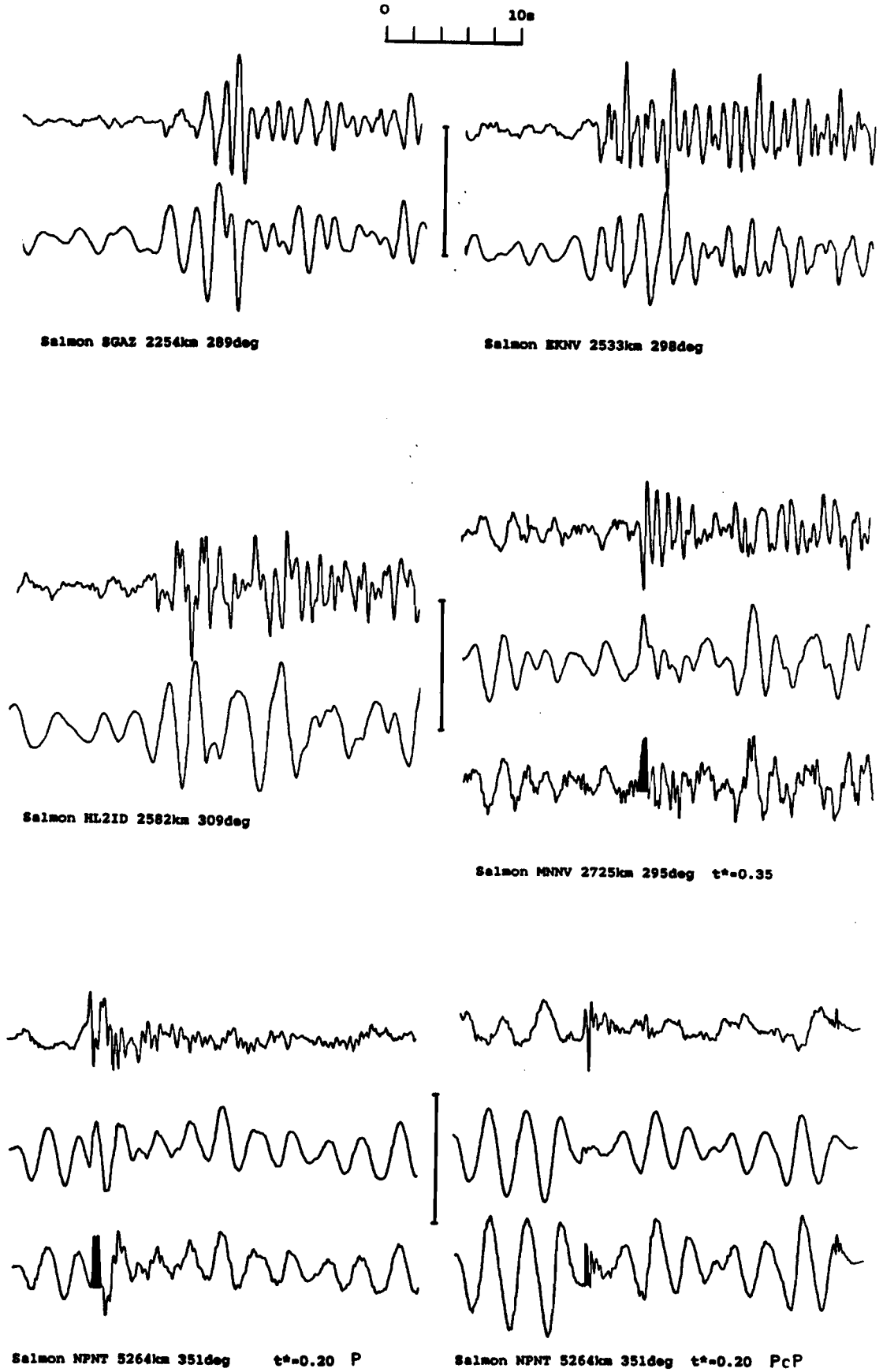

Fig 5c. SP,BB & t* corrected BB seismograms for SALMON

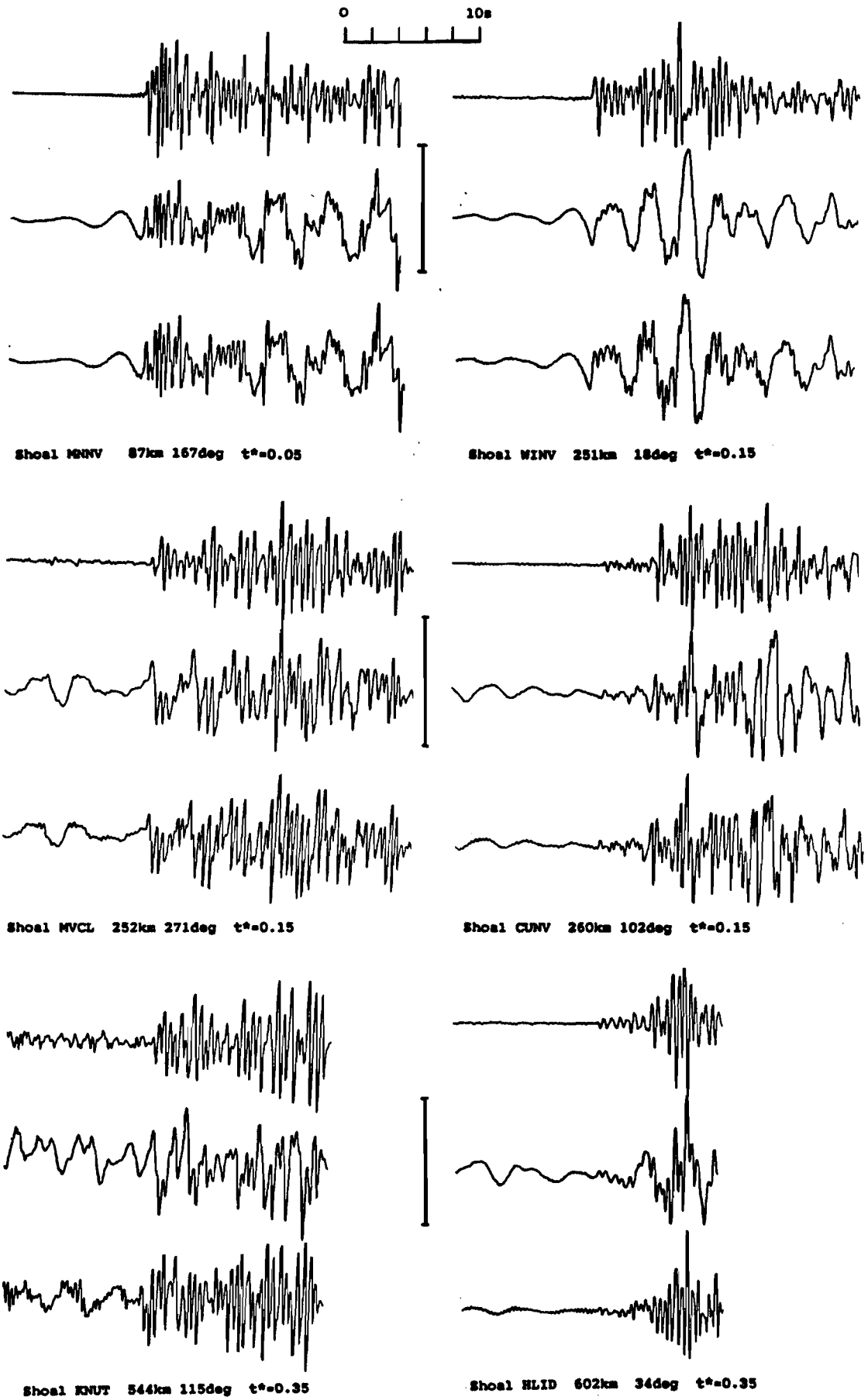

Fig 6a. SP,BB & t* corrected BB seismograms for SHOAL

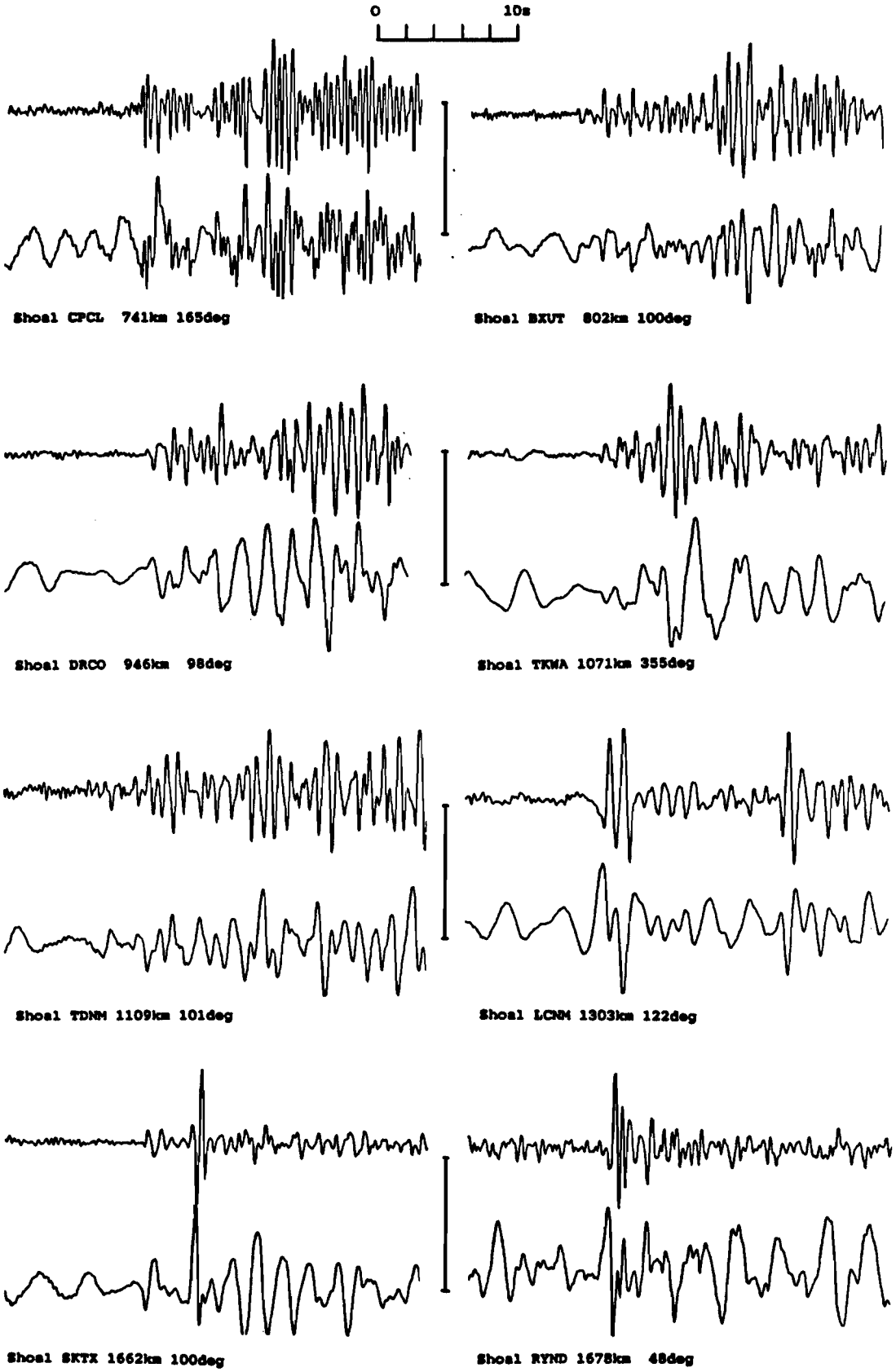

Fig 6b. SP,BB & t* corrected BB seismograms for SHOAL

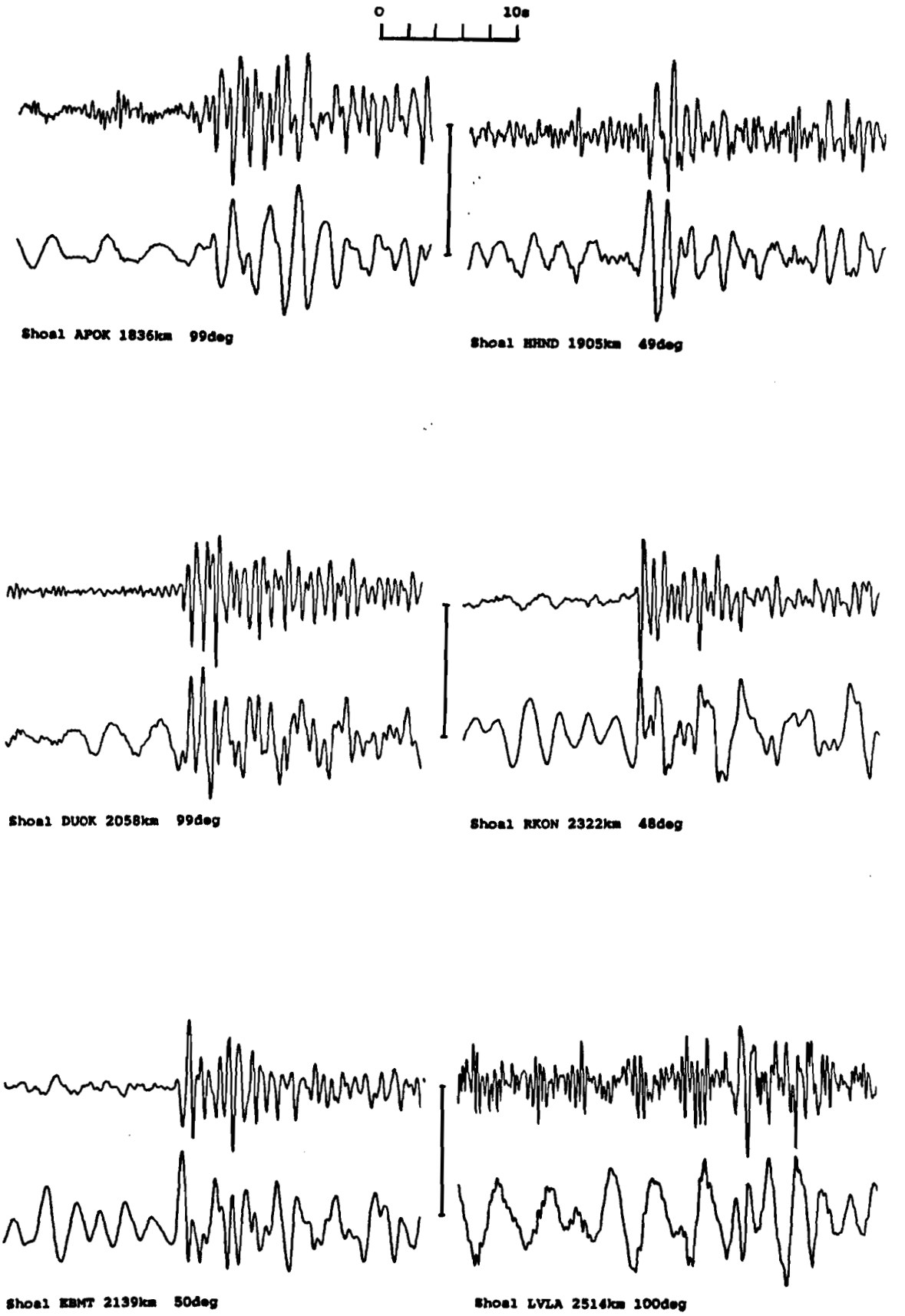

Fig 6c. SP,BB & t* corrected BB seismograms for SHOAL

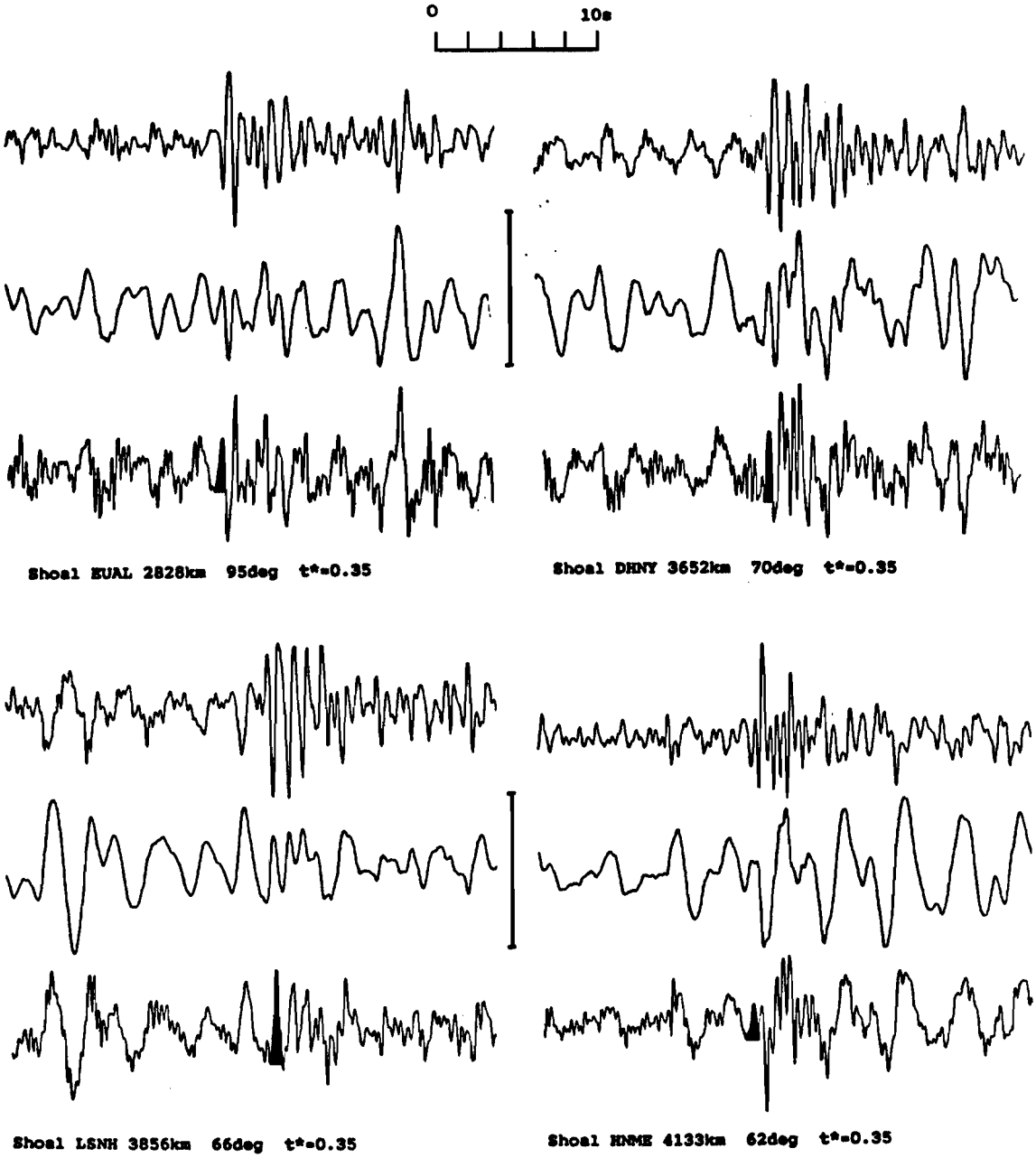

Fig 6d. SP,BB & t* corrected BB seismograms for SHOAL

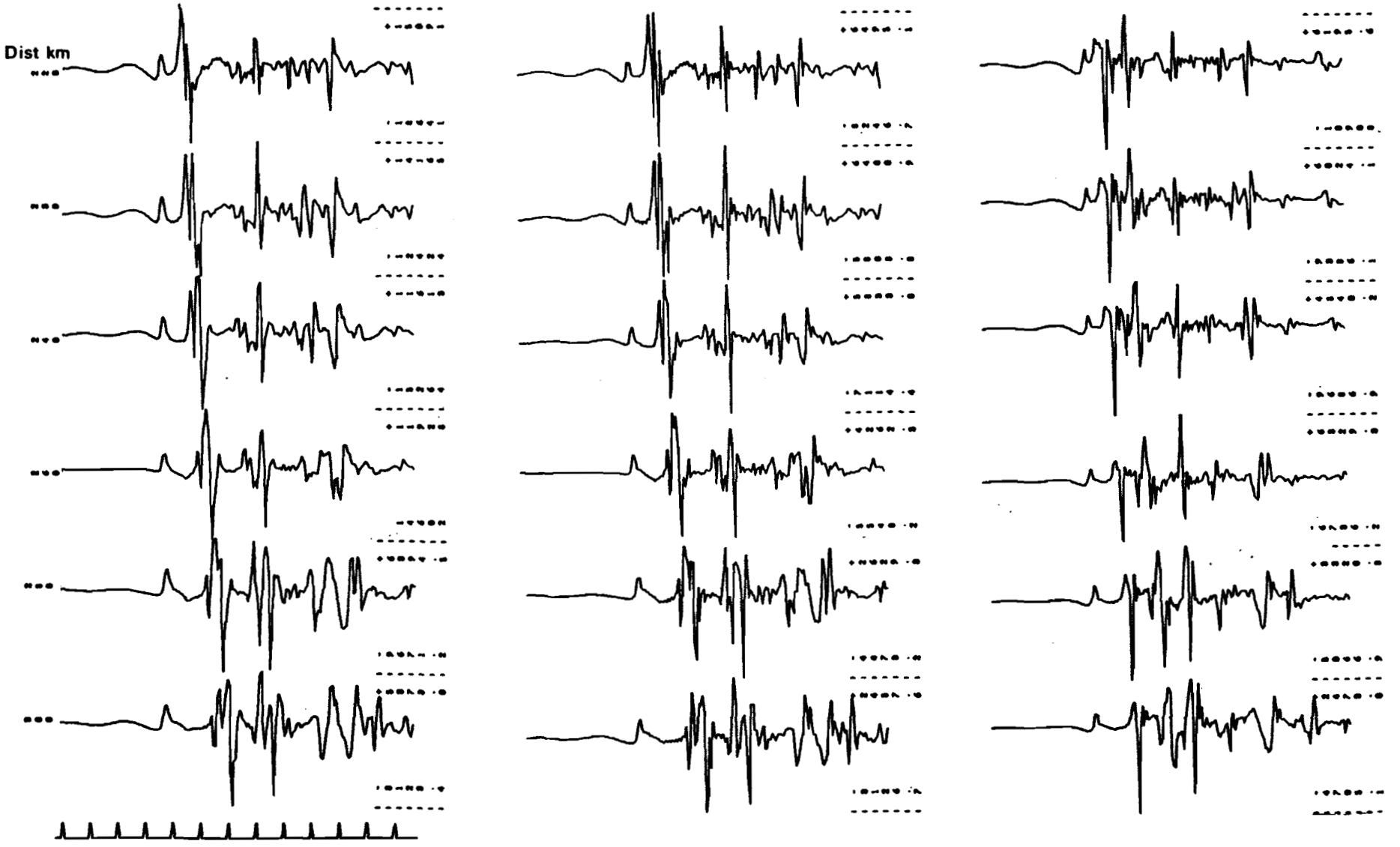

FIG 7. Theoretical BB seismograms for explosion PILEDRIVER for the distance range 220-300km. Source waveforms are based on the Mueller-Murphy model assuming source medium details given table 1. Seismograms to the left & centre are based on structure A in table 3 and yields of 62 & 20 kt repectively. The seismograms to the right are for 20kt and the structure modified by reducing the depth to the lower crustal layer by 10km. Numbers to right are max & min amplitudes in nm. Time marks are every 2 seconds.

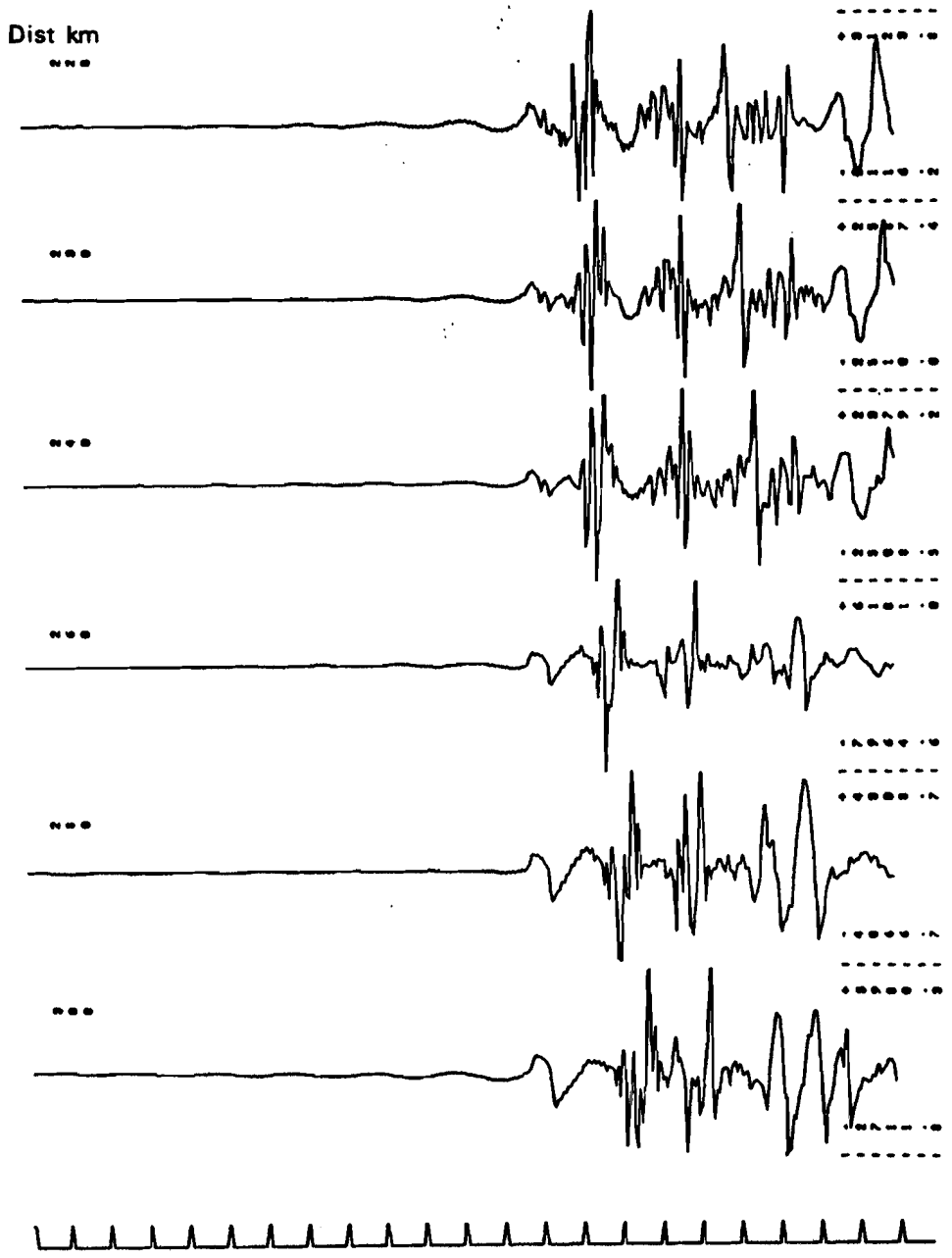

FIG 8. Theoretical seismograms for a double couple source 2.5km depth in structure A in table 3. The double couple corresponds to a slip angle of 115° on a fault plane with strike 120° & dip 140°. The top three seismograms are for the azimuth and distance range corresponding to station MNNV from PILEDRIVER. The bottom three are for station KNUT. Source waveform is assumed to be an impulse and ψinf arbitrarily set to 10000 cubic metres. Numbers to right are max & min amplitudes in nm Time marks every 2 seconds.

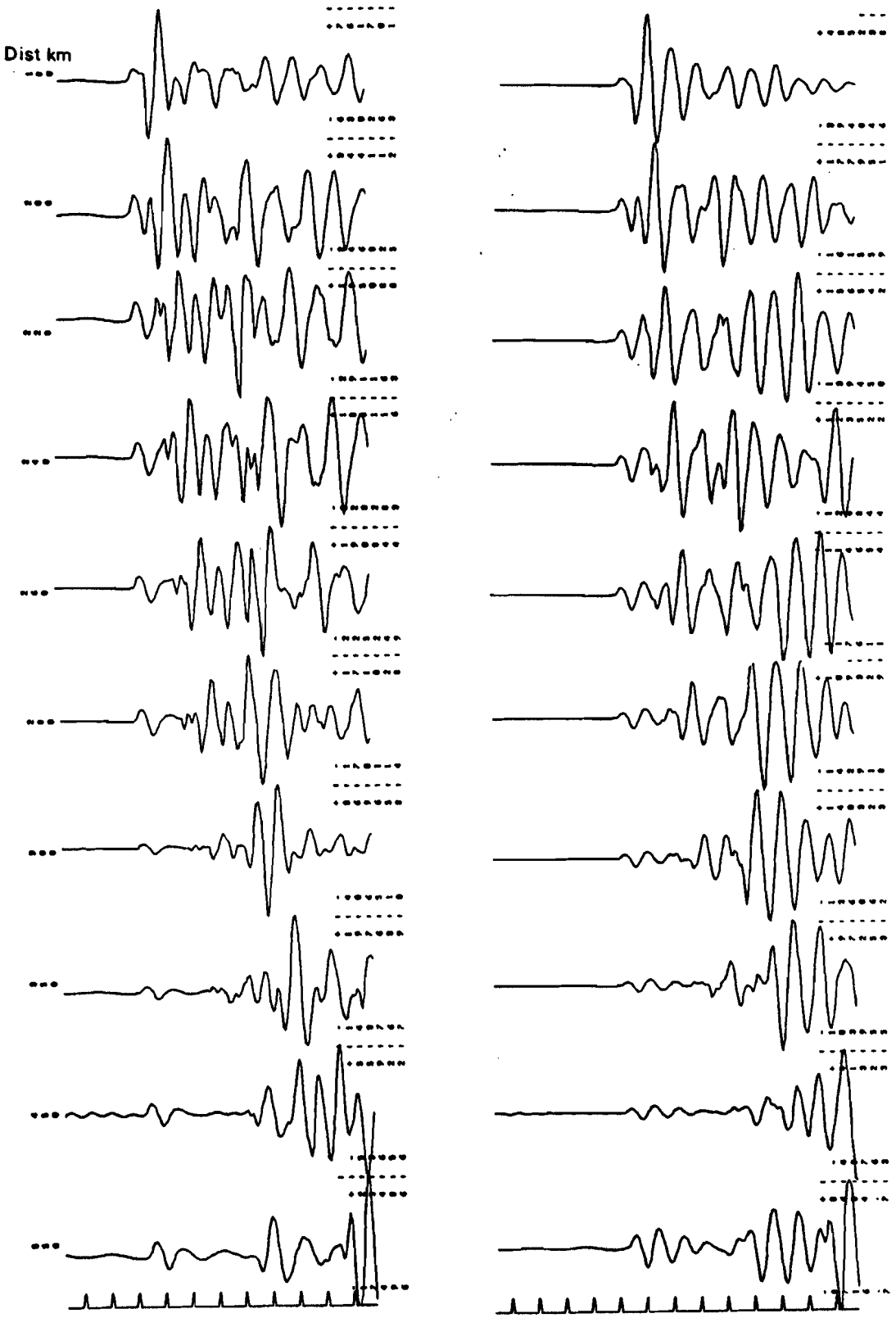

FIG 9. Theoretical seismograms over the distance range 180-550km for explosions BILBY (right) & BOXCAR (left). Source waveforms based on the Mueller-Murphy model assuming source medium details, depths & yields given in table 1. Earth structures used are B & C in table 3 correspond to NTS Yucca flats & Pahute mesa respectively. Numbers to the right are max & min amplitudes in nm. Time marks every 2 seconds.

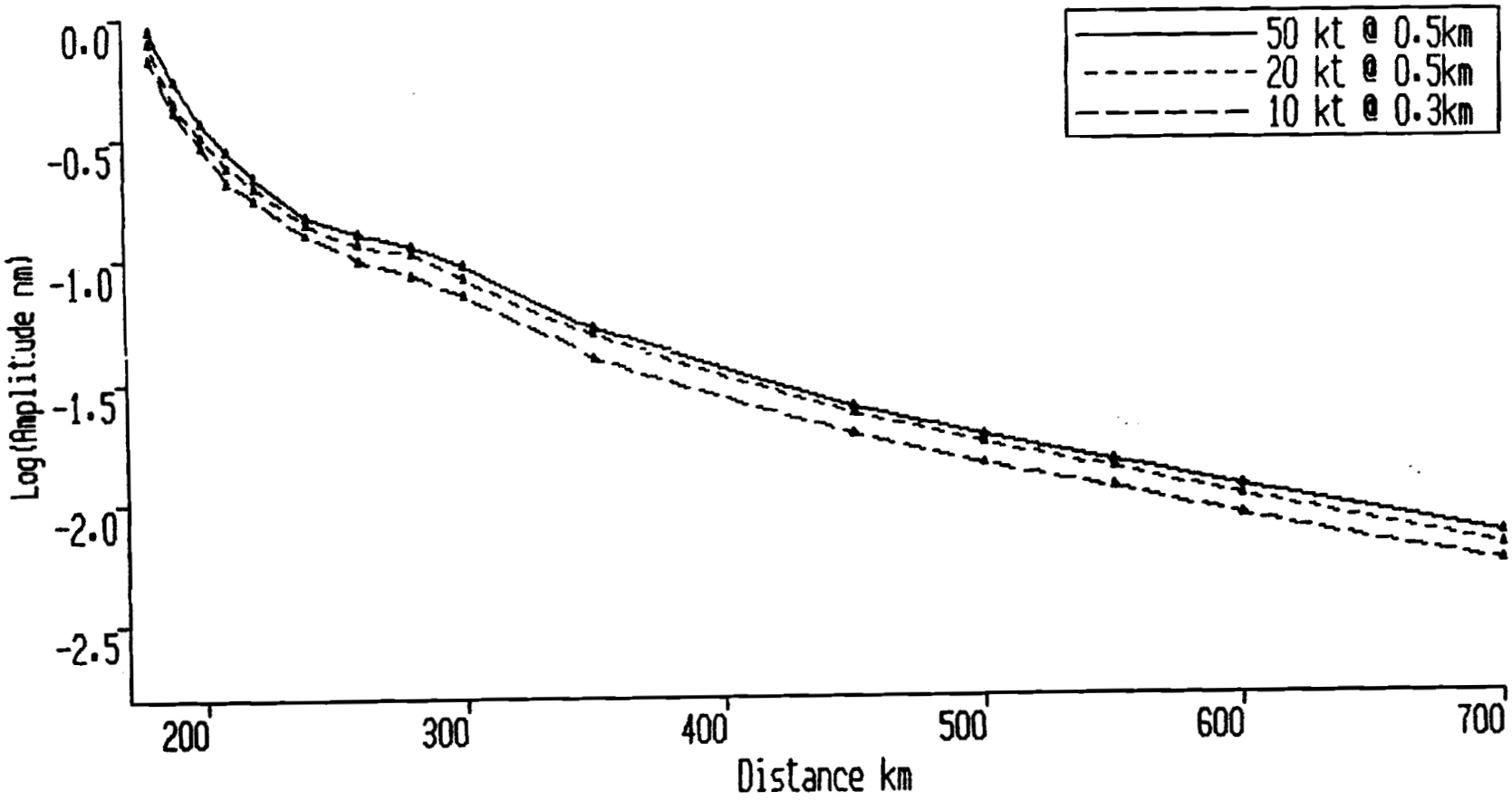

FIG 10. Amplitude in nm of the Pn BB arrival corresponding to sources with peak RDP of 1 cubic metre. Amplitudes are measured from theoretical seismograms for sources in the NTS granitic structure A table 3. Source waveforms are based on the Mueller-Murphy model for yields and depths indicated.

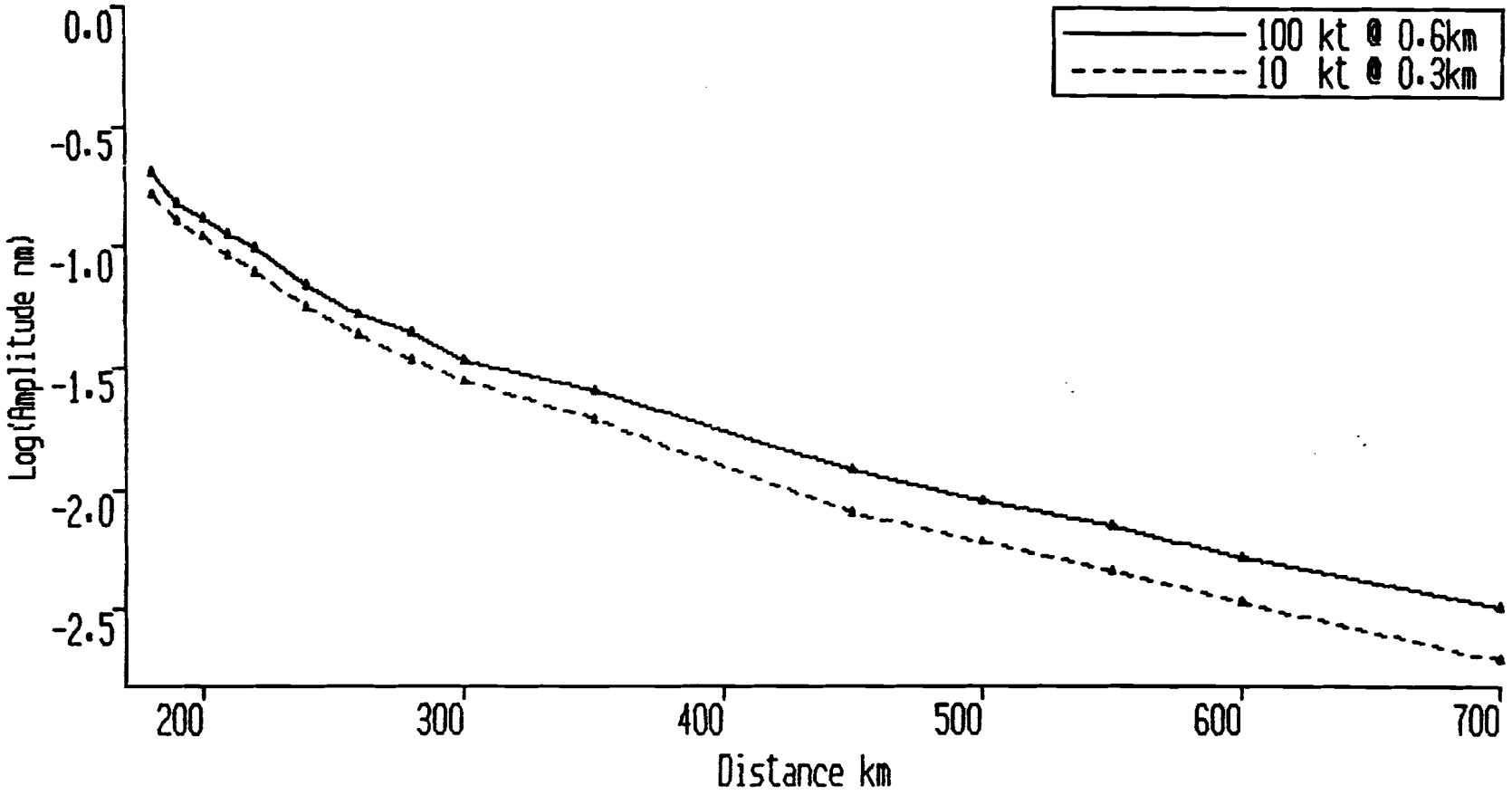

FIG 11. Amplitude in nm of the Pn BB arrival corresponding to sources with peak RDP of 1 cubic metre. Amplitudes are measured from theoretical seismograms for sources in the NTS Yucca flats structure B table 3. Source waveforms are based on the Mueller-Murphy model for yields and depths indicated.

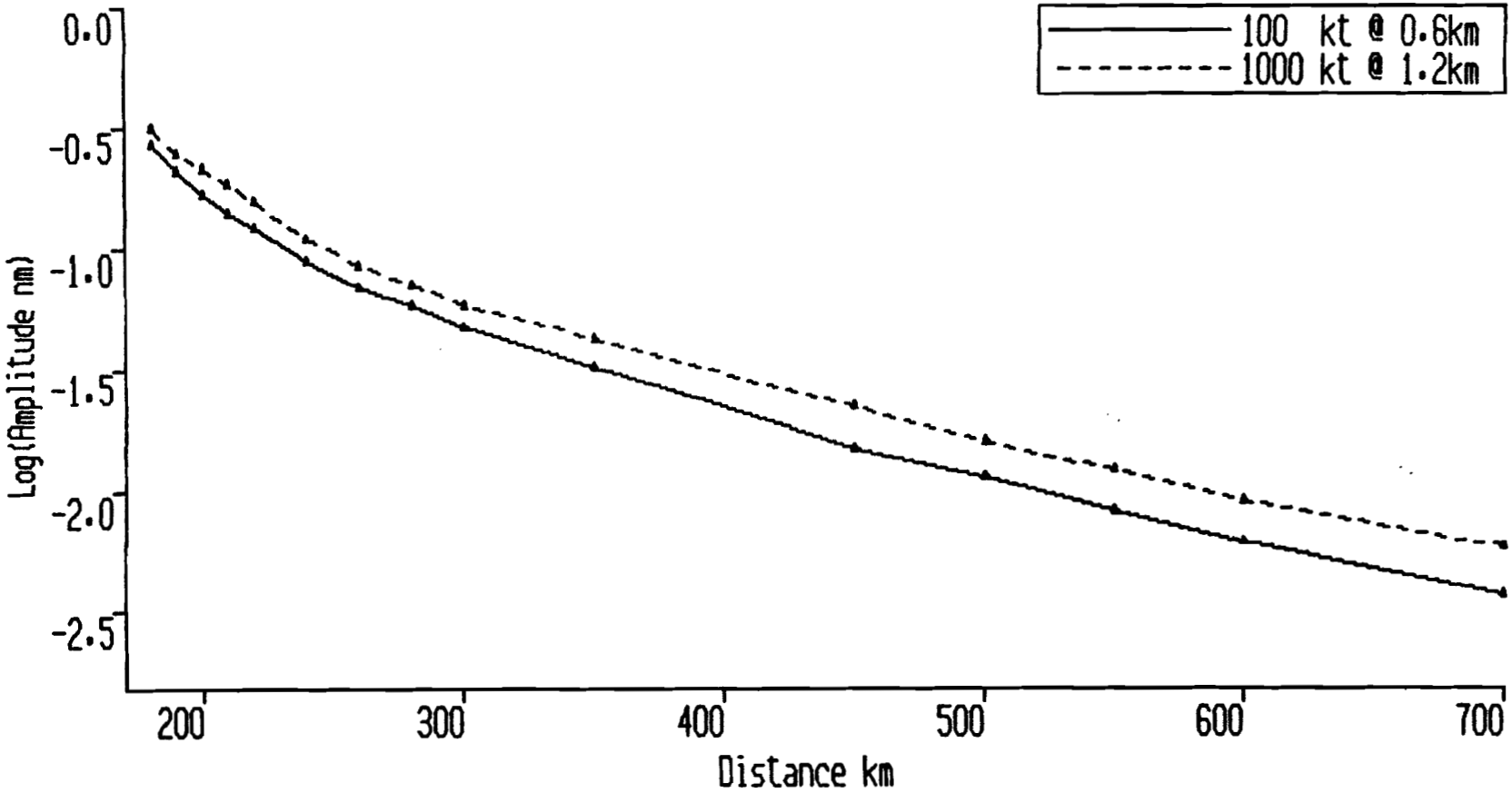

FIG 12. Amplitude in nm of the Pn BB arrival corresponding to sources with peak RDP of 1 cubic metre. Amplitudes are measured from theoretical seismograms for sources in the NTS Pahute mesa structure C table 3. Source waveforms are based on the Mueller-Murphy model for yields and depths indicated.

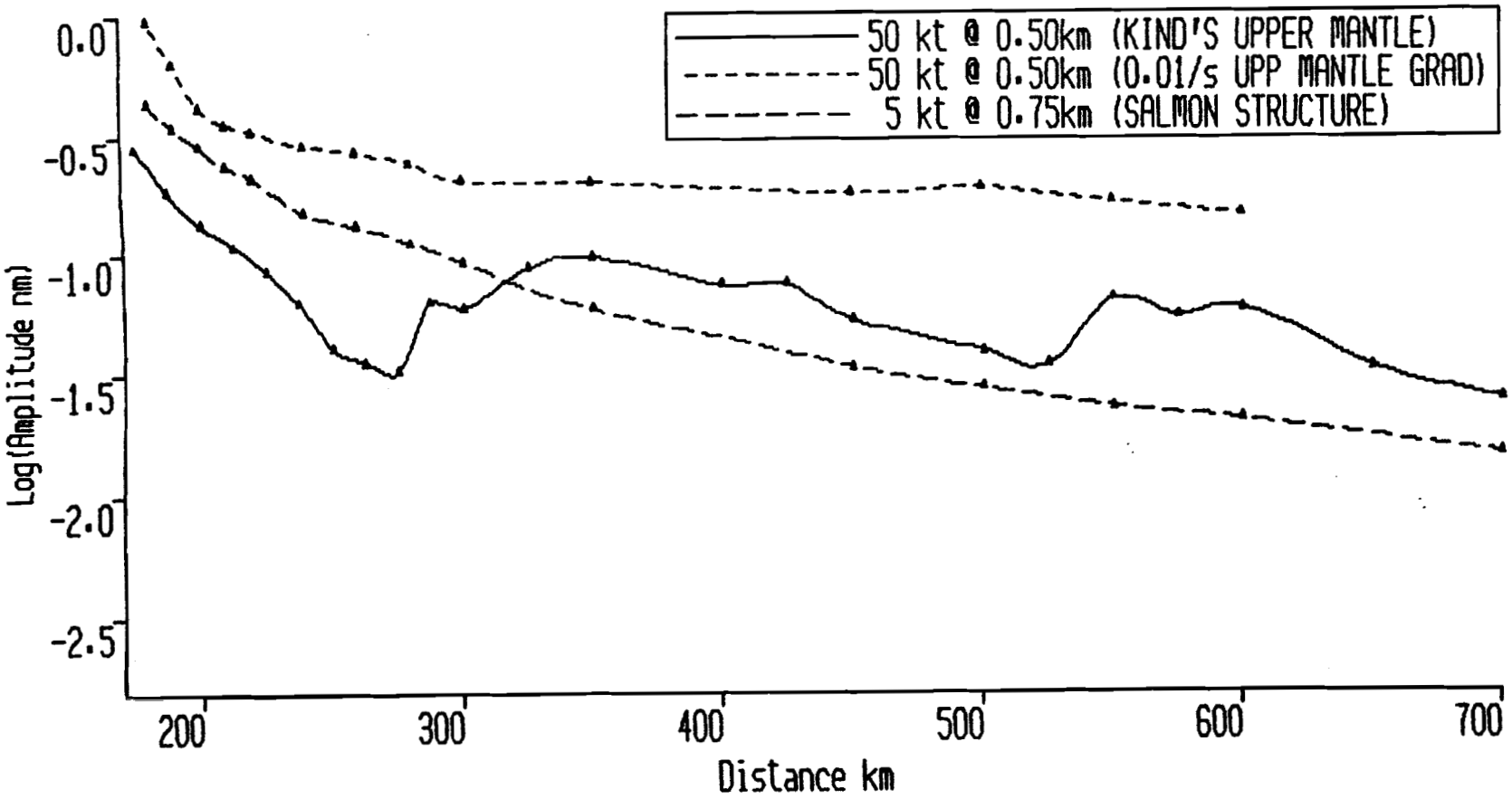

FIG 13. Amplitude in nm of the Pn BB arrival corresponding to sources with peak RDP of 1 cubic metre. Amplitudes are measured from theoretical seismograms for sources in the Salmon structure D, high gadient structure E and Kind's structure F in table 3. Source waveforms are based on the Mueller-Murphy model for yields and depths indicated.

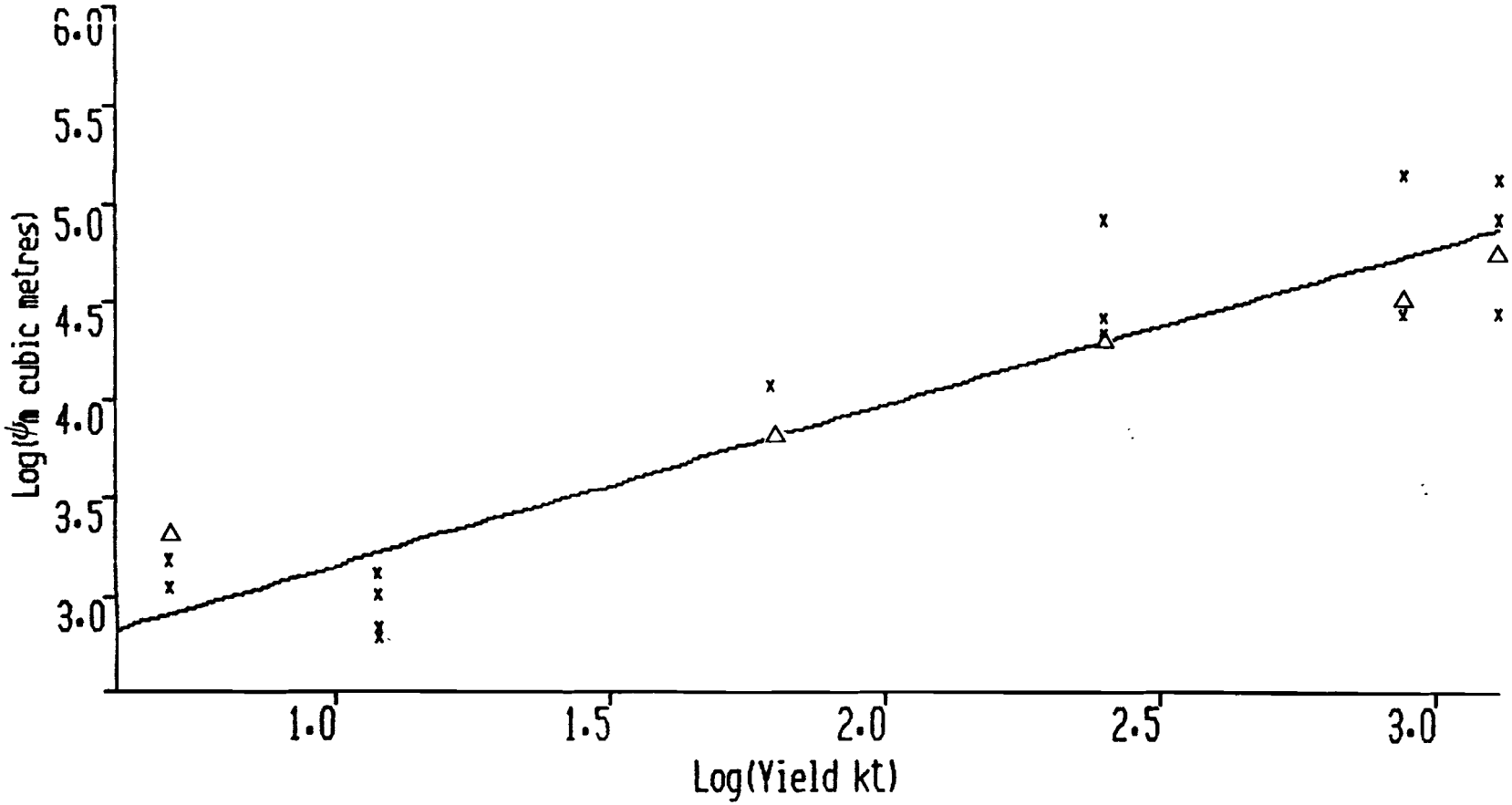

FIG 14. Plot of Log(ψ_m) measured using teleseismic data against Log(Yield) for the six shots studied in this report. Crosses are measurements using LRSM stations(this report) Triangles are from refs (1,4,24). Regression line has form Log(ψ_m)=2.33+0.82Log(Yield). ψ_m is in cubic metres & Yield in Kilotons.

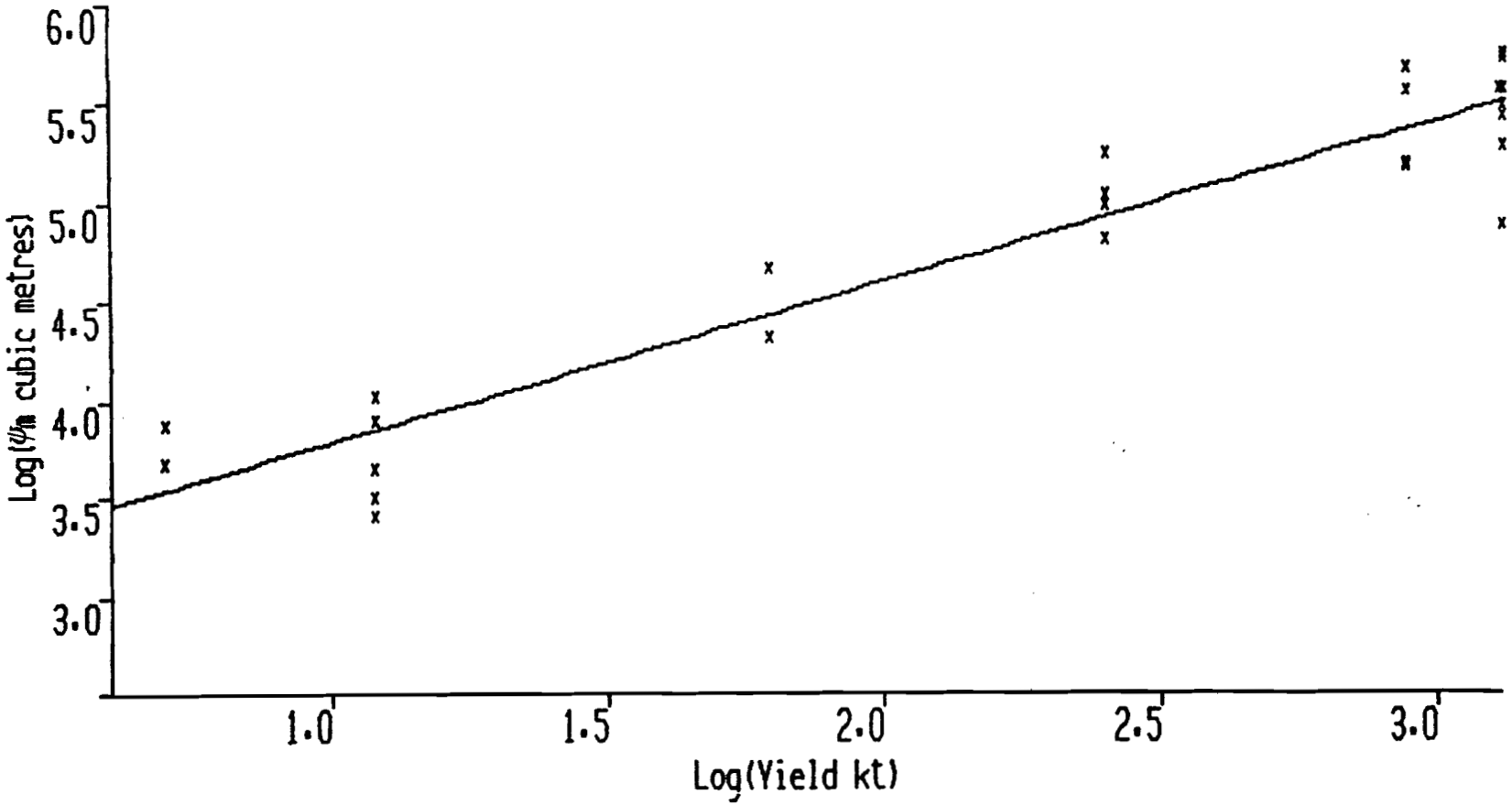

FIG 15. Plot of Log(ψ_m) measured using the Pn arrival against Log(Yield) for the six shots studied in this report. Regression line has form Log(ψ_m)=2.97+0.82Log(Yield). ψ_m is in cubic metres & Yield in Kilotons.

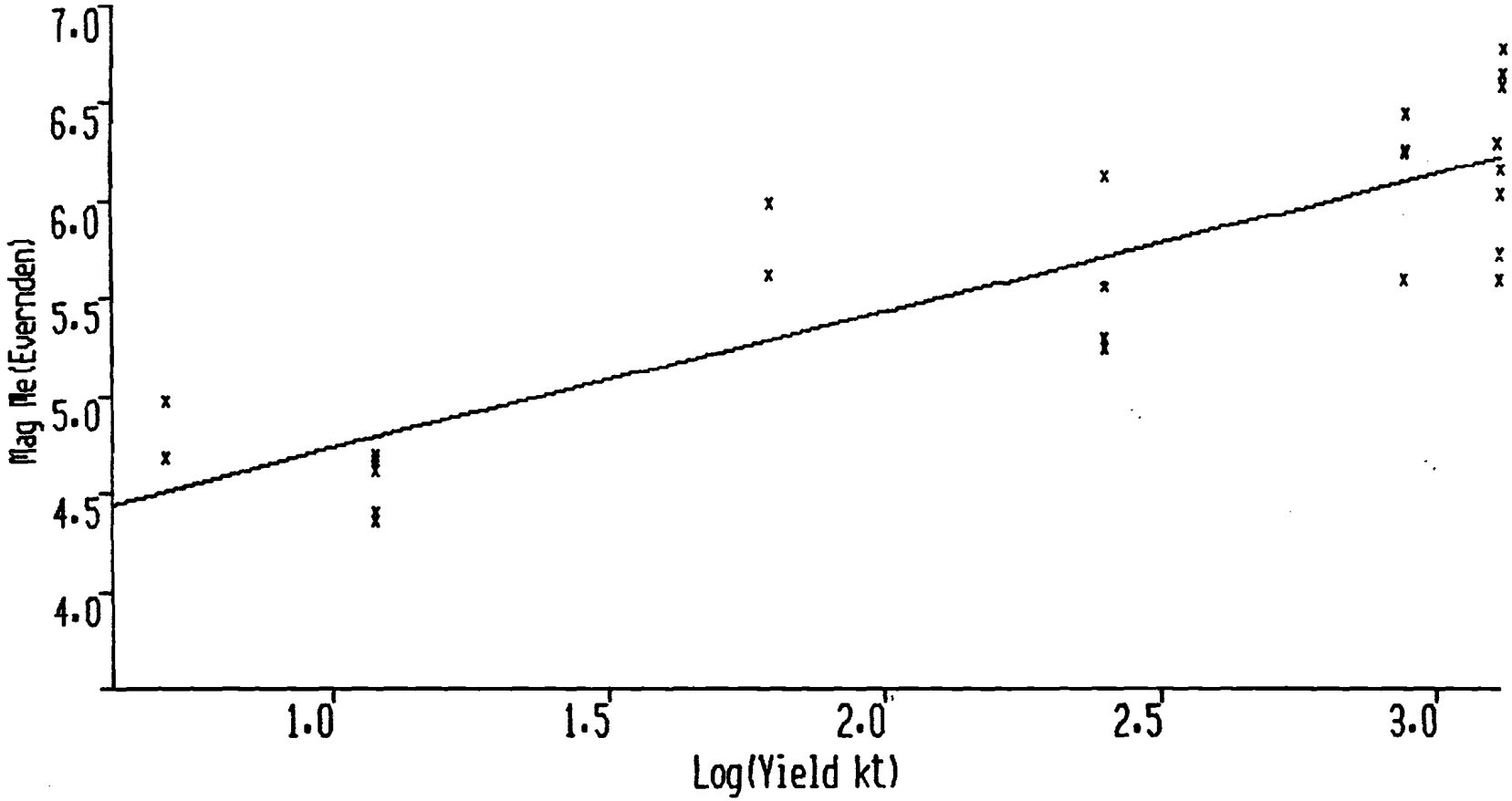

FIG 16. Plot of Magnitude against Log(Yield) for the six shots studied in this report. Magnitude is based on Pn log(A/T) measurements taken from LRSM shot reports(refs 25-30) and corrections for distance published by Evernden(31). Yield is in Kilotons. Regression line has form M=4.02+0.71Log(Yield).

Available from
HER MAJESTY'S STATIONERY OFFICE
49 High Holborn, London W.C.1
71 Lothian Road, Edinburgh EH3 9AZ
9-12 Princess Street, Manchester M60 8AS
Southey House, Wine Street, Bristol BS1 2BQ
258 Broad Street, Birmingham B1 2HE
80 Chichester Street, Belfast BT1 4JY
or through any bookseller.

Printed in England

ISBN 85518188 5

UK UNLIMITED